

Macrophage IL-10 Blocks CD8⁺ T Cell-Dependent Responses to Chemotherapy by Suppressing IL-12 Expression in Intratumoral Dendritic Cells

Brian Ruffell,¹ Debbie Chang-Strachan,^{2,6} Vivien Chan,² Alexander Rosenbusch,^{1,3} Christine M.T. Ho,¹ Nancy Pryer,² Dylan Daniel,² E. Shelley Hwang,⁴ Hope S. Rugo,⁵ and Lisa M. Coussens^{1,*}

¹Department of Cell, Developmental & Cancer Biology and Knight Cancer Institute, Oregon Health & Science University, Portland, OR 97239, USA

²Novartis Institutes for Biomedical Research, Emeryville, CA 94608, USA

³Friedrich-Alexander-Universität Erlangen-Nürnberg, 91054 Erlangen, Germany

⁴Surgery Department, Duke University, Durham, NC 27708, USA

⁵Department of Medicine and Helen Diller Family Comprehensive Cancer Center, University of California, San Francisco, San Francisco, CA 94143, USA

⁶Present address: Cellerant Therapeutics, San Carlos, CA 94070, USA

*Correspondence: cousseni@ohsu.edu

<http://dx.doi.org/10.1016/j.ccell.2014.09.006>

SUMMARY

Blockade of colony-stimulating factor-1 (CSF-1) limits macrophage infiltration and improves response of mammary carcinomas to chemotherapy. Herein we identify interleukin (IL)-10 expression by macrophages as the critical mediator of this phenotype. Infiltrating macrophages were the primary source of IL-10 within tumors, and therapeutic blockade of IL-10 receptor (IL-10R) was equivalent to CSF-1 neutralization in enhancing primary tumor response to paclitaxel and carboplatin. Improved response to chemotherapy was CD8⁺ T cell-dependent, but IL-10 did not directly suppress CD8⁺ T cells or alter macrophage polarization. Instead, IL-10R blockade increased intratumoral dendritic cell expression of IL-12, which was necessary for improved outcomes. In human breast cancer, expression of *IL12A* and cytotoxic effector molecules were predictive of pathological complete response rates to paclitaxel.

INTRODUCTION

Tumor-associated macrophages are associated with poor clinical outcome in most carcinomas, with clinical and preclinical data indicating that this is due largely to macrophage promotion of angiogenesis, local invasion, and increased metastatic capacity (Bingle et al., 2002; Ruffell et al., 2012a). Because macrophages are highly dependent on the colony-stimulating factor-1 (CSF-1) and CSF-1 receptor (CSF-1R) pathway for survival in most tissues (Pollard, 2009), there is significant interest in therapeutically targeting this pathway. In murine models, small-molecule inhibitors of CSF-1R induce tumor regression

in glioblastoma multiforme (Pyonteck et al., 2013), prevent tumor growth in cervical cancer (Strachan et al., 2013), and partially delay growth of implanted melanoma cell lines (Mok et al., 2014). An α CSF-1R monoclonal antibody (mAb) has also demonstrated clinical efficacy in diffuse-type giant tumors, a disease driven by overexpression of CSF-1 and recruitment of myeloid cells (Ries et al., 2014).

In the mouse mammary tumor virus (MMTV)-polyoma middle T (PyMT) transgenic model of luminal B-type mammary carcinoma, tumor infiltration by F4/80⁺ macrophages parallels disease progression (DeNardo et al., 2009), and MMTV-PyMT mice harboring homozygous null mutations in the CSF-1 gene

Significance

Therapeutics targeting the CSF-1/CSF-1 receptor pathway are currently being evaluated clinically in multiple cancer types, either as monotherapy or in combination with standard-of-care chemotherapy. However, mechanisms by which the CSF-1/CSF-1 receptor pathway and macrophages sustain tumor growth and/or repress response to cytotoxic therapy are unclear. Herein we report that macrophages infiltrating mammary carcinomas are the significant source of IL-10, which in turn suppresses intratumoral dendritic cell production of IL-12 and thereby limits cytotoxic T cell responses during chemotherapy. These data reveal a role for the interaction between tumor macrophages and dendritic cells in mediating response to therapy, identify a CSF-1/IL-10/IL-12 cytokine axis for targetable intervention, and reveal possible risk stratification biomarkers for patient selection.

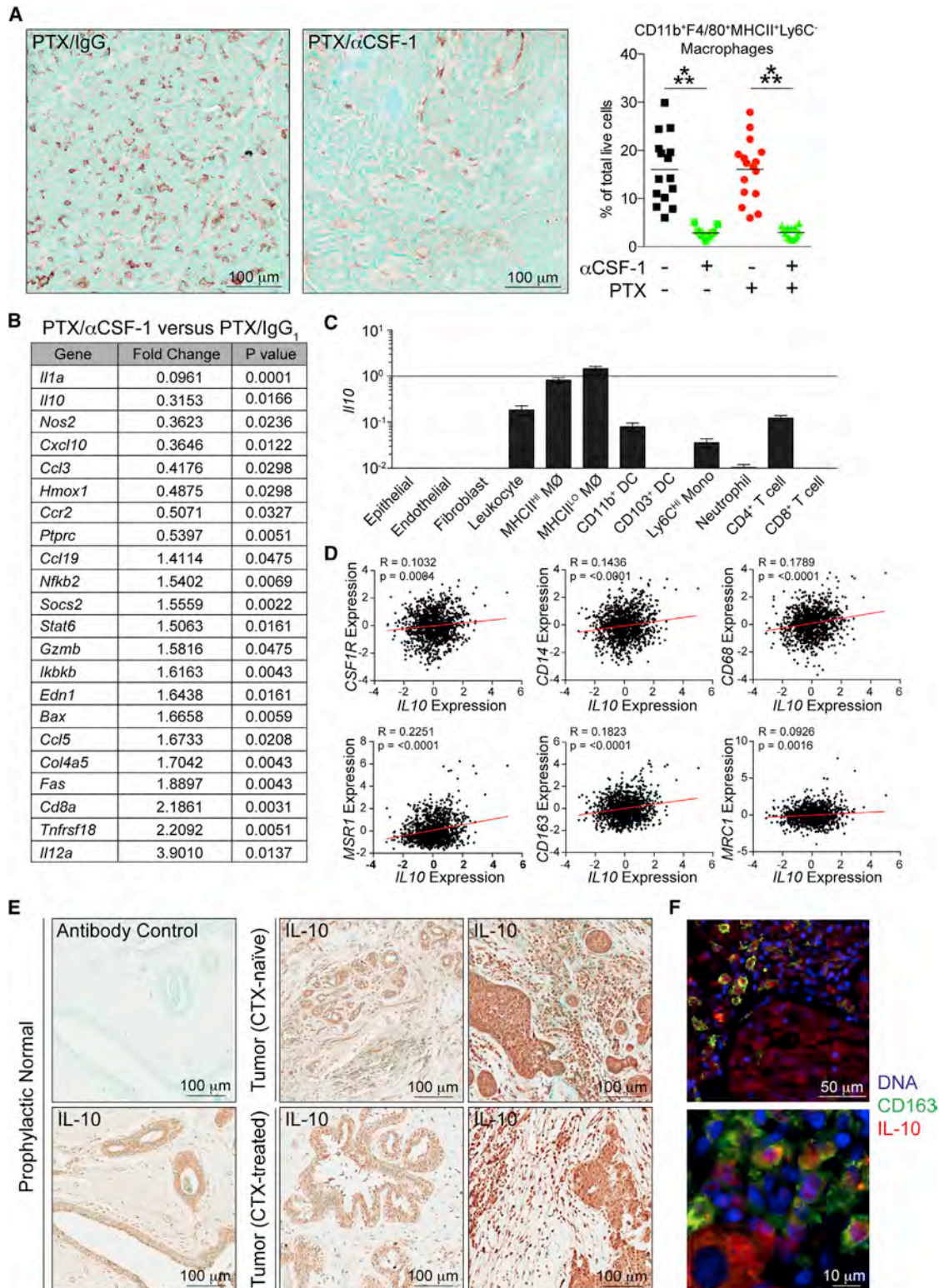


Figure 1. Macrophages Are the Primary Source of IL-10 in Mammary Tumors

(A) Representative images of F4/80 immunoreactivity (left) in mammary tumors from MMTV-PyMT mice treated with IgG₁ or α CSF-1 mAb in combination with PTX. Quantitation of CD11b⁺F4/80⁺MHCII⁺Ly6C⁻ macrophages by flow cytometry is shown to the right as a percentage of total live cells. Significance was determined by an unpaired t test with Welch's correction, with ***p < 0.001.

(legend continued on next page)

exhibit limited tumor angiogenesis, slowed tumor progression, and inhibited pulmonary metastasis (Lin et al., 2001). Although therapeutic depletion of macrophages from tumors with mAbs or small-molecule inhibitors targeting CSF-1 or CSF-1R, respectively, exhibits no efficacy as single agents (DeNardo et al., 2011; Strachan et al., 2013), administration in combination with standard-of-care chemotherapy (CTX) significantly slows primary tumor growth kinetics and diminishes pulmonary metastasis (DeNardo et al., 2011). On the basis of these data, clinical studies combining the CSF-1R small-molecule inhibitor PLX3397 and CTX are currently under way (ClinicalTrials.gov identifiers NCT01596751 and NCT01525602).

Although macrophages have been found to directly promote the survival of mammary carcinoma cells in a cathepsin-dependent manner in vitro (Shree et al., 2011), our previous studies reported that enhanced chemotherapeutic efficacy associated with CSF-1R inhibition was dependent on cytotoxic CD8⁺ T cells (DeNardo et al., 2011), thus indicating a role for macrophages in suppressing a T cell response during CTX. Several studies have demonstrated that tumor-associated macrophages directly suppress CD8⁺ T cell activation in vitro (DeNardo et al., 2011; Doedens et al., 2010; Movahedi et al., 2010), and CSF-1R inhibition has been found to enhance adoptive cell transfer therapy in melanoma models (Mok et al., 2014). However, the mechanism(s) by which macrophages suppress antitumor responses, either directly or indirectly in vivo, remains unclear. Here we sought to inform ongoing clinical trials by delineating functionally significant mechanisms whereby tumor-infiltrating macrophages suppress CD8⁺ T cell responses during CTX.

RESULTS

Macrophages Are the Primary Source of Interleukin-10 in Mammary Carcinomas

To identify the molecular mechanisms by which macrophages limited response to CTX in mammary carcinomas, we effectively depleted macrophages through administration of α CSF-1 mAb in combination with paclitaxel (PTX) in MMTV-PyMT tumor-bearing mice (Figure 1A) and examined the status of tumor vasculature (Figures S1A and S1B available online), as well as expression of immune-related genes in whole tumor tissue (Figure 1B). Although macrophages promote formation of abnormal tumor vasculature (Stockmann et al., 2008), we did not observe changes in density of CD31⁺ vessels, the ratio of pericytes to endothelial cells, or extravasation of either doxorubicin or PTX into mammary tumors, as quantitatively evaluated by immunofluorescence approaches or liquid chromatography-mass spec-

troscopy, respectively (Figures S1C and S1D), thus indicating that improved responses to CTX were unlikely linked to improved tumor hemodynamics. Instead, gene expression data revealed decreases in several myeloid-associated genes relative to control tissue, including *Il1a*, *Il10*, *Nos2*, *Cxcl10*, *Ccl3*, and *Ccr2*, and, inversely, increased expression of *Gzmb*, *Ccl5*, *Cd8a*, and *Il12a*, consistent with our previous report of a role for CD8⁺ T cells in mediating response to CTX following CSF-1R inhibition (DeNardo et al., 2011). We found no change in genes reflecting a CD4/T_H1 response (*Irfng*, *Tbx21*, and *Cd4*).

Of the mRNAs exhibiting reduced expression following α CSF-1 mAb therapy, *Il10* is the most strongly associated with an established immunosuppressive role in vivo (Moore et al., 2001). We confirmed macrophages as the primary source of interleukin (IL)-10 in untreated mammary carcinomas by evaluating fluorescence-activated cell-sorted epithelial versus stromal cell populations (Figures S1E and S1F). *Il10* expression was limited to CD45⁺ leukocytes, with expression observed in Ly6C⁺ monocytes, CD11b⁺ dendritic cells (DCs), CD4⁺ T cells, and F4/80⁺ macrophages (Figure 1C). Macrophage expression of *Il10* was approximately 10-fold higher than other leukocyte populations, with an additional ~1.5-fold average increase in expression by MHCII^{LO} versus MHCII^{HI} macrophages. We further characterized the MHCII^{HI} and MHCII^{LO} macrophage subsets and found that both were effectively depleted by α CSF-1 mAb treatment (Figures S1G–S1I), and exhibited similar nuclear morphology in cytopins (Figure S1J); however, MHCII^{LO} macrophages displayed increased expression of several markers associated with T_H2/M2-type programming at both the protein (MSR1, MRC1, and IL4R α) (Figure S1K) and mRNA (*Cd163*, *Msr1*, *Mrc1*, *Il4ra*, *Arg1*, and *Ptgs2*) levels (Figure S1L).

On the basis of high expression of *Il10* by macrophages, and its partial correlation with M2/T_H2-type biomarkers in mammary carcinomas, we evaluated expression of *IL10* in human breast cancer samples from The Cancer Genome Atlas (TCGA) data set against genes associated with presence of myeloid cells (*CSF1R*, *CD14*, and *CD68*) or macrophage polarization (*MSR1*, *MRC1*, and *CD163*). We identified significant correlation between these mRNAs, with the most significant correlation occurring for *MSR1* and *CD163* (Figure 1D). *IL10* expression did not correlate with *FOXP3* expression (data not shown), despite reports of regulatory T (T_{Reg}) cells being a critical source of IL-10 in some murine tumor models (Stewart et al., 2013). Because the association between *IL10* expression and macrophage markers was relatively weak ($R < 0.23$), we also evaluated the presence of IL-10 protein by immunohistochemistry in human breast cancer samples. In accordance with the gene expression correlations, we observed high expression within stromal cells,

(B) Fold change in whole-tissue gene expression in tumors from PTX/ α CSF-1 mAb-treated mice determined by real-time PCR using a 96-gene immune array. Only significant ($p < 0.05$; Mann-Whitney test) changes are shown; $n \geq 12$ mice per group.

(C) *Il10* mRNA expression levels from fluorescence-activated cell-sorted stromal populations isolated from untreated mice as determined by real time PCR. Data are normalized to *Tbp* expression and displayed as mean \pm SEM with $n = 8$ per cell type. M ϕ , macrophage; mono, monocyte.

(D) Correlation between *IL10* expression and various myeloid-associated genes in human breast cancer samples from the TCGA data set ($n = 1,161$).

(E) Detection of IL-10 in human breast cancer by immunohistochemistry. Fourteen CTX-naive and 9 CTX-treated patient samples were evaluated. Representative images reflecting low and high staining are displayed.

(F) Immunofluorescent staining for IL-10, CD163, and DNA using Hoescht 33342 in human breast cancer. Representative images from one of three patient samples are displayed.

See also Figure S1.

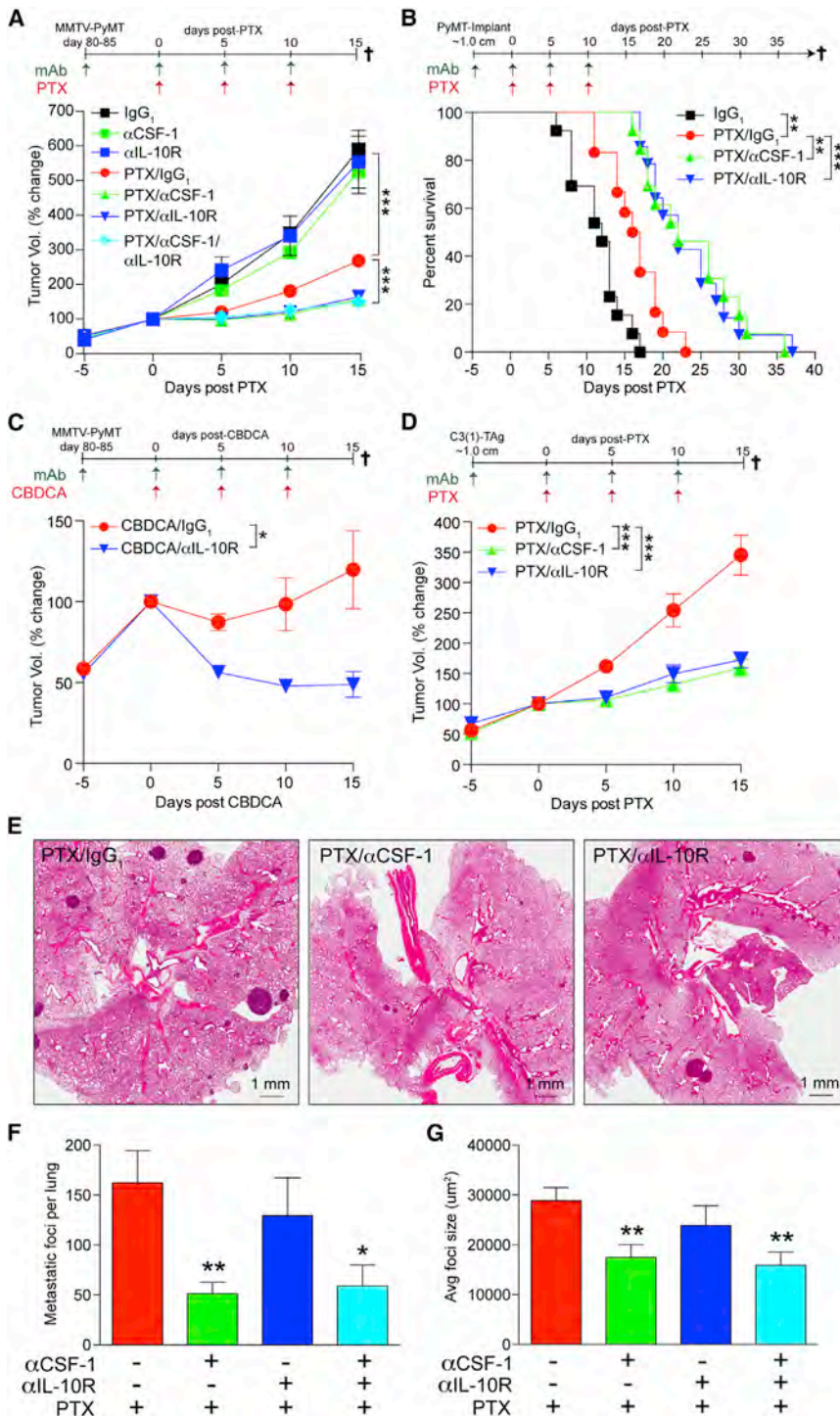


Figure 2. IL-10 Receptor Blockade Improves Response to PTX

(A) Relative tumor volume in MMTV-PyMT mice following treatment with IgG₁, αCSF-1 mAb, αIL-10R mAb, PTX, or a combination thereof. Dosing strategy is displayed at top. Data are displayed as mean ± SEM, with n ≥ 9 mice per group. Significance was determined by two-way ANOVA, with ***p < 0.001.

(B) Survival of mice bearing orthotopic PyMT-derived tumor explant tumors following treatment with IgG₁, αCSF-1 mAb, αIL-10R mAb, PTX, or a combination thereof. Significance was determined by log rank, with **p < 0.01 and ***p < 0.001; n ≥ 12 mice per group.

(C) Relative tumor volume in MMTV-PyMT mice following treatment with IgG₁ or αIL-10R mAb in combination with carboplatin (CBDCA). Dosing strategy is displayed at top. Data are displayed as mean ± SEM, with n ≥ 5 mice per group. Significance was determined by two-way ANOVA, with *p < 0.05.

(D) Relative tumor volume in C3(1)-TAG mice following treatment with IgG₁, αCSF-1 mAb, or αIL-10R mAb in combination with PTX. Dosing strategy is displayed at top. Data are displayed as mean ± SEM, with n ≥ 8 mice per group. Significance was determined by two-way ANOVA, with ***p < 0.001.

(E) Representative hematoxylin and eosin sections of lungs taken from animals treated with PTX alone or in combination with αCSF-1 mAb or αIL-10R mAb.

(F) The number of metastatic foci per lung in each treatment group from (A). Data are displayed as mean ± SEM, with n ≥ 9 mice per group. Significance was determined by an unpaired t test with Welch's correction, with *p < 0.05 and **p < 0.01. (G) The average size of metastatic foci in each treatment group. Data are displayed as mean ± SEM, with n ≥ 9 mice per group. Significance was determined by an unpaired t test with Welch's correction with **p < 0.01. See also Figure S2.

Blockade of the IL-10 Receptor Improves Response to PTX

To examine whether IL-10 was functionally relevant for regulating response to CTX, we treated late-stage tumor-bearing MMTV-PyMT mice with an IL-10 receptor-blocking mAb (αIL-10R; clone 1B1.3A) prior to and throughout a chemotherapeutic regimen of 10 mg/kg PTX administered every 5 days (Figure 2A).

including CD163⁺ cells with a myeloid morphology (Figures 1E and 1F). In contrast to murine tumor tissue, however, we also observed variable expression within tumor epithelial cells. Thus, although macrophages, in particular T_H2/M2-type macrophages, are associated with expression of IL-10 in both murine mammary carcinomas and human breast cancer, IL-10 production within human breast tumors displays increased variability and complexity.

Although neither αIL-10R nor αCSF-1 mAb alone altered tumor growth kinetics relative to control mice over this time period, combinatorial PTX with either mAb significantly slowed tumor growth more effectively than PTX alone, with significant growth differences occurring following the second dose of PTX. No additional improvement was observed by combining αCSF-1 and αIL-10R mAbs plus PTX. Using a syngeneic orthotopic implantable PyMT explant model to evaluate survival, we

observed greater than 2-fold increased survival with either α CSF-1 mAb/PTX or α IL-10R mAb/PTX (10 days) following initiation of treatment at approximately 1.0 cm in average tumor diameter, compared with mice treated with PTX alone (4.5 days) (Figure 2B). MMTV-PyMT mice treated with α IL-10R mAb also displayed an enhanced response to 50 mg/kg carboplatin (CBDCA), with tumors regressing approximately 50% over the course of treatment (Figure 2C). Using the C3(1)-TAG model of triple negative mammary carcinogenesis (Deeb et al., 2007; Maroulakou et al., 1994) we also found significant diminution of primary tumor growth when combining PTX with either α CSF-1 or α IL-10R mAbs (Figure 2D; Figures S2A–S2C). Thus, the ability of IL-10 to limit chemotherapeutic efficacy was not limited by the type of chemotherapeutic or the subtype of mammary carcinoma being examined.

Regarding pulmonary metastasis, whereas α CSF-1 mAb/PTX diminished both the number and size of metastatic foci in MMTV-PyMT mice (Figures 2E–2G), inclusion of α IL-10R mAb in this regimen yielded no additional benefit. Neither α CSF-1 nor α IL-10R mAbs caused changes to proliferating cells (BrdU positivity) or cell death (cleaved caspase-3 positivity) in metastatic foci beyond that observed with PTX alone (Figure S2D). Our interpretation of these data was that whereas CSF-1R-activated macrophages produce epidermal growth factor (EGF) that in turn fosters neoplastic mammary epithelial cell invasion and metastasis (DeNardo et al., 2009; Lin et al., 2001), macrophage-derived IL-10 was not involved in programs regulating metastasis and instead represented a macrophage-dependent pathway within primary tumors regulating response to CTX.

Because a significant clinical issue theoretically limiting efficacy of CSF-1/CSF-1R-targeted therapy is perceived liver toxicity due to reduced density of liver Kupffer cells (Strachan et al., 2013; Wei et al., 2005), we evaluated overall health of mice enrolled in these studies by several criteria. As expected, on the basis of a role for Kupffer cells in clearance of serum enzymes (Radi et al., 2011), we observed increased serum alkaline phosphatase, alanine aminotransferase, and aspartate aminotransferase (Figure S2E) following α CSF-1 mAb therapy. Similar to what has been reported in nonhuman primates and rodents (Radi et al., 2011), however, neutralizing CSF-1 alone or in combination yielded no adverse effects on animal health with respect to liver pathology, weight loss, or renal toxicity (Figures S2F–S2H). No changes in animal health were noted with α IL-10R mAb alone or in combination. Thus, targeting of either IL-10R or CSF-1 improved efficacy of PTX without evidence of acute toxicity.

Improved Response to PTX Is CD8⁺ T Cell Dependent

To reveal mechanisms whereby macrophage IL-10 regulated response to CTX, we examined the presence of T cell populations in mammary tumors either 2 or 5 days following the final dose of PTX. Five days after PTX, α CSF-1 mAb or α CSF-1 mAb/PTX resulted in a small increase in the presence of CD4⁺FoxP3⁺ T_{Reg} cells, with no significant changes observed in CD4⁺FoxP3⁻ T_H cells or CD8⁺ T cells (Figure S3A). In contrast, in mammary tumors evaluated 2 days after PTX, α CSF-1 mAb and α CSF-1 mAb/PTX therapy resulted in a significant increase in the relative frequency of CD8⁺ T cells (Figure 3A). Because this change may have resulted from depletion of the major leuko-

cyte population, we also evaluated the relative frequency of CD4⁺ T_H cells and found no significant alteration in most groups (Figure 3B), resulting in an increased CD8/CD4 T cell ratio within tumors from α CSF-1 mAb treated animals (Figure 3C). No changes were observed in CD4⁺ or CD8⁺ T cell infiltration following α IL-10R mAb or α IL-10R mAb/PTX therapy at either time point. Because increased CD8⁺ T cell infiltration was observed with α CSF-1 mAb even in the absence of CTX, and α CSF-1 mAb/PTX treatment increased mRNA expression of *Gzmb* in whole tissue (Figure 1B), we evaluated whether any of the combinatorial therapies increased the density of granzyme B (GZMB)-expressing cells, indicative of perhaps a “better” cytotoxic T lymphocyte response. Indeed, both α CSF-1 mAb/PTX and α IL-10R mAb/PTX therapy increased tumor density of GZMB-positive cells 2 days after PTX by approximately 1.5-fold (Figure 3D). Increased presence of GZMB-positive cells was significant as CD8-depletion prior to PTX ablated improved outcomes for tumor-bearing mice treated with α IL-10R mAb/PTX therapy (Figure 3E), similar to our previous finding using a CSF-1R antagonist (DeNardo et al., 2011).

IL-10 Does Not Influence Macrophage Recruitment, Polarization, or Function

Because macrophages are known to express IL-10R, we examined whether IL-10R-blockade was directly influencing macrophage presence or function in mammary tumors. Whereas α CSF-1 mAb led to reduced presence of the two predominant populations of macrophages (i.e., MHCII^{hi} and MHCII^{lo}) in mammary carcinomas (Figures 4A and 4B), blockade of IL-10R exerted no similar impact (Figures 4A and 4B), as well as having no effect on the presence of monocytes or neutrophils in tumors (Figures 4C and 4D).

Because macrophages isolated from MMTV-PyMT mammary tumors have been reported to exert immunosuppressive activity *ex vivo* (DeNardo et al., 2011; Doedens et al., 2010), we next evaluated the role of IL-10 in mediating this activity. Notably, the ability of tumor-infiltrating macrophages to suppress splenic CD8⁺ T cell proliferation *in vitro* was largely isolated to the MHCII^{lo} population (Figures 4E and 4F), correlating with the presence of MHCII^{lo} macrophages in areas of tumor hypoxia *in situ* (Figure 4G) and higher expression of *Arg1* (Figure S1L), similar to models of lung carcinogenesis (Laoui et al., 2014; Movahedi et al., 2010). That said, neither α IL-10 neutralizing nor α IL-10R blocking mAb altered the immunosuppressive capacity of the MHCII^{hi} or MHCII^{lo} macrophage subset *ex vivo* (Figure 4H), and concordantly, addition of IL-10 did not suppress proliferation or expression of GZMB, interferon (IFN)- γ , or tumor necrosis factor- α by CD8⁺ splenocytes during *in vitro* stimulation (Figures S3B–S3E). On the basis of these data, and the fact that IL-10 can promote IL-2-induced proliferation of human (Groux et al., 1998) and mouse CD8⁺ T cells (Chen and Zlotnik, 1991) when used at high concentrations (100 U/ml), we concluded that macrophage-derived IL-10 was likely regulating CD8⁺ T cell functionality indirectly. This conclusion was bolstered by the fact that gene expression programs in macrophages isolated from tumor-bearing mice treated with α IL-10R mAb were only modestly altered (Figure S4), with the exception of reduced expression of *Socs3*, a downstream target gene of IL-10R signaling (Figure 4I).

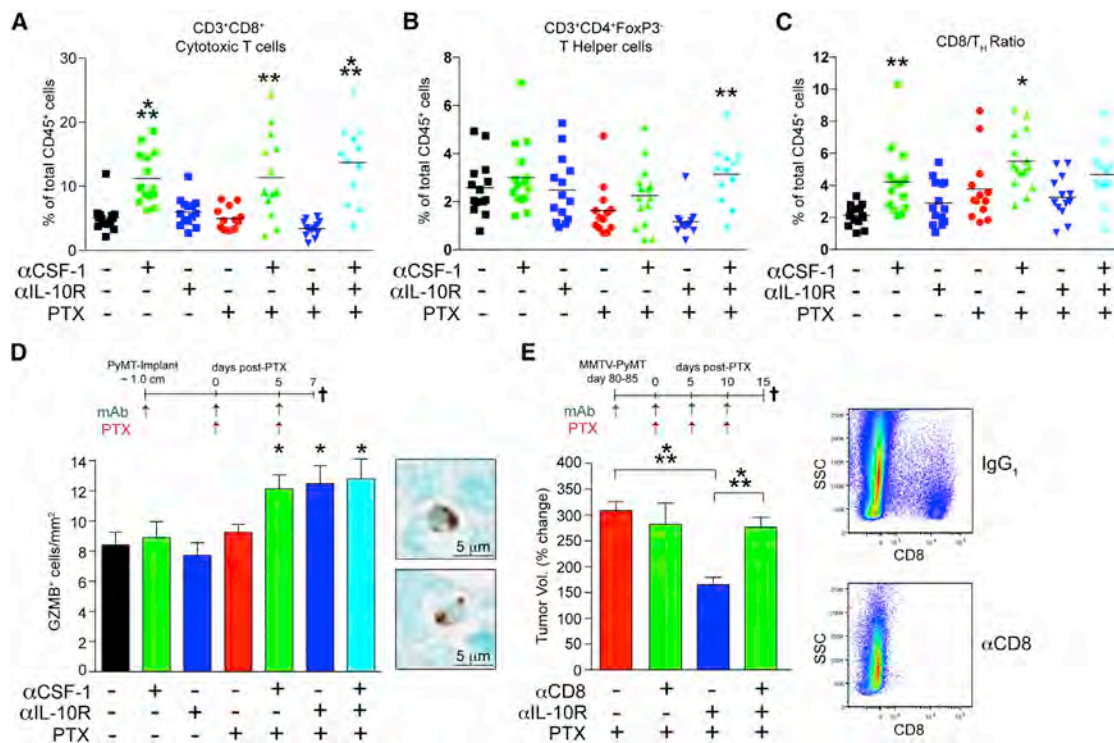


Figure 3. Response to α IL-10R/PTX Is CD8⁺ T Cell Dependent

(A–C) Flow cytometric quantitation of CD3⁺CD8⁺ cytotoxic T cells (A), CD3⁺CD4⁺FoxP3⁺ T_H cells (B), and ratio of CD8⁺ to CD4⁺ T_H cells (C) in orthotopic PyMT-derived tumors 2 days following the second dose of PTX (day 7). Significance was determined by an unpaired t test with Welch's correction relative to IgG₁ or IgG₁/PTX control groups, with **p* < 0.05, ***p* < 0.01, and ****p* < 0.001.

(D) Density of GZMB-expressing cells in orthotopic PyMT-derived tumors on day 7 as determined by immunohistochemistry. Data are displayed as mean ± SEM, with *n* ≥ 12 mice per group. Significance was determined by an unpaired t test with Welch's correction relative to IgG₁ or IgG₁/PTX control groups, with **p* < 0.05. Representative images are shown to the right.

(E) Relative mammary tumor volume after 3 rounds of PTX in MMTV-PyMT transgenic mice following treatment with α IL-10R mAb and PTX. CD8⁺ T cells were depleted 5 days prior to the first dose of PTX. Data are displayed as mean ± SEM, with *n* ≥ 5 mice per group. Significance was determined by an unpaired t test with ****p* < 0.001. Polychromatic dot plots displaying CD8⁺ T cell depletion are shown to the right.

See also Figure S3.

Dendritic Cells Express High Levels of IL-10R

To address this hypothesis and identify cells infiltrating mammary tumors that potentially were being regulated by macrophage-derived IL-10, we evaluated expression patterns of IL-10R by flow cytometry. Although IL-10R expression has been observed on colonic epithelium (Denning et al., 2000), the IL-10-binding subunit of IL-10R (IL-10R α /IL-10R1) was restricted to CD45⁺ leukocytes in mammary tumors, with the exception of low expression by platelet-derived growth factor receptor α (PDGFR α)⁺ fibroblasts (Figure 5A). To identify select lineages contributing to CD45⁺ expression, we isolated leukocyte subsets from mammary tumors as compared with equivalent populations from spleens (where possible) of non-tumor-bearing mice (Figure 5B). These data revealed significantly increased expression of IL-10R on CD4⁺ T cells, Ly6C^{HI} monocytes, macrophages, and DCs, specifically CD103[−]CD11b⁺ and CD103⁺CD11b[−] DC subsets, in tumors, with no significant increased expression on CD8⁺ T cells compared with normal spleen (Figure 5B).

On the basis of these findings, we hypothesized that increased expression of IL-10R on select myeloid cells indicated their potential role in regulating functional CD8⁺ T cell responses

following CTX in response to macrophage-derived IL-10. Because α IL-10R mAb therapy did not alter presence of macrophages or monocytes in tumors (Figures 4A–4C) and did not significantly alter macrophage gene expression programs (Figure S4), we evaluated the relative percentage of DCs infiltrating tumors from the various experimental groups. As shown in Figure 5C, there was an ~1.5-fold increase in CD103[−]CD11b⁺ DCs in tumors from both α CSF-1 mAb/PTX and α IL-10R mAb/PTX treatment groups, with a further ~3-fold increased presence in tumors from α CSF-1 mAb/ α IL-10R mAb/PTX-treated mice, compared with PTX alone. CD103⁺CD11b[−] DCs were also increased by either α CSF-1 mAb/PTX or α IL-10R mAb/PTX treatment, although the effects of α CSF-1 mAb/PTX were more significant (Figure 5C). Immunofluorescent staining of carcinomas revealed that CD103⁺ cells (reflecting populations of DCs and CD8⁺ T cells) were dispersed throughout tumor stroma in proximity to F4/80⁺ macrophages, with limited invasion of the tumor parenchyma (Figure 5D). Although the density of CD103⁺ cells was increased by α CSF-1 mAb/PTX treatment, their localization appeared unchanged (Figure 5D).

Because tumor macrophages and tumor DCs both express CD11c, albeit with higher surface expression by DCs

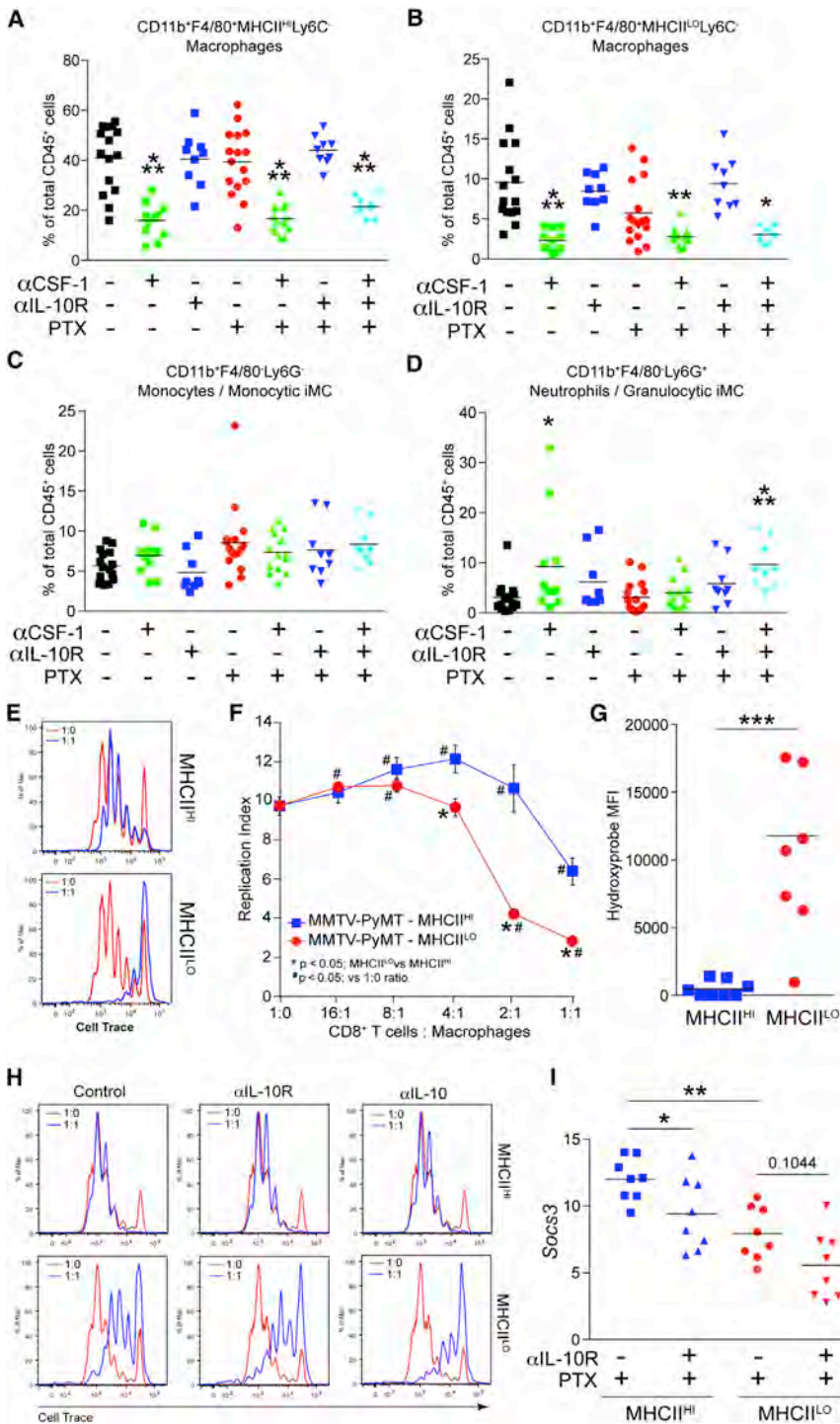


Figure 4. IL-10 Does Not Influence Macrophage Recruitment, Polarization, or Function

(A–D) Percentage of total CD45⁺ cells in mammary tumors composed of CD11b⁺F4/80⁺MHCII^{HI}Ly6C⁻ macrophages (A), CD11b⁺F4/80⁺MHCII^{LO}Ly6C⁻ macrophages (B), CD11b⁺F480⁺Ly6G⁻ monocytes (C), and CD11b⁺F4/80⁺Ly6G⁺ neutrophils (D). Data were generated by flow cytometry. Significance was determined by an unpaired t test with Welch’s correction relative to IgG₁ or IgG₁/PTX control groups, with *p < 0.05, **p < 0.01, and ***p < 0.001.

(E) Representative histograms displaying cell trace fluorescence of CD8⁺ splenic T cells stimulated with αCD3/αCD28 for 60 hr either alone (red) or cocultured (blue) at a 1:1 ratio with fluorescence-activated cell-sorted MHCII^{HI} or MHCII^{LO} macrophages from mammary carcinomas.

(F) Fold expansion of dividing CD8⁺ T cells (replication index) is displayed at various ratios of CD8⁺ T cells to macrophages as described in (E). One of two experiments is shown, with samples assayed in triplicate. Data are displayed as mean ± SEM.

(G) Detection of hydroxyprobe (pimonidazole) by intracellular staining of tumor-associated macrophages. Significance was determined by an unpaired t test with Welch’s correction, with ***p < 0.001.

(H) Representative histograms displaying cell trace fluorescence of CD8⁺ splenic T cells as described in (E), with addition of 10 μg/ml αIL-10R or αIL-10 mAb added at the start of the incubation period. One of two experiments is shown.

(I) Socs3 expression in MHCII^{HI} and MHCII^{LO} tumor macrophage subsets determined by real-time PCR, with data analyzed by comparative threshold cycle method using *Tbp* as a reference gene. Significance was determined by Mann-Whitney test, with *p < 0.05 and **p < 0.01. See also Figure S4.

(Figure S1K), we fluorescence-activated cell-sorted tumor macrophages, DCs, monocytes, and neutrophils to affirm the correct populations had been isolated (Figure S5). Confirming our gating strategy, CD11b⁺ and CD103⁺ DCs displayed preferential expression of DC transcription factors (e.g., *Zbtb46*, *Ciita*, and *Pvrl1*) and surface markers (e.g., *Ccr7*, *Flt3*, *Notch2*, and *Cd26*) compared with either MHCII^{HI} or MHCII^{LO} macrophage populations.

Along with the increase in DC infiltration observed following either αIL-10R mAb/PTX or αCSF-1 mAb/PTX therapy (Figure 5C), we noted an almost 4-fold increase in *Ii12a* expression in tumors from αCSF-1 mAb/PTX-treated mice (Figure 1B). Because CD8⁺ T cells in MMTV-PyMT mammary tumors expressed both subunits of the IL-12 receptor (Figures S6A and S6B), and IL-12 is known to enhance CD8⁺ T cell proliferation and effector function (Trinchieri, 2003), we investigated a possible role for IL-10 in regulating IL-12 production by DCs and thereby influencing CD8⁺ T cell responses during CTX. To evaluate this, we first examined mRNA expression of the IL-12 subunits in sorted leukocyte populations. In mammary tumors from untreated mice, expression of *Ii12a* mRNA was observed in most populations; however, mRNA expression of the p40 subunit of IL-12 (*Ii12b*) was limited to DCs and macrophages

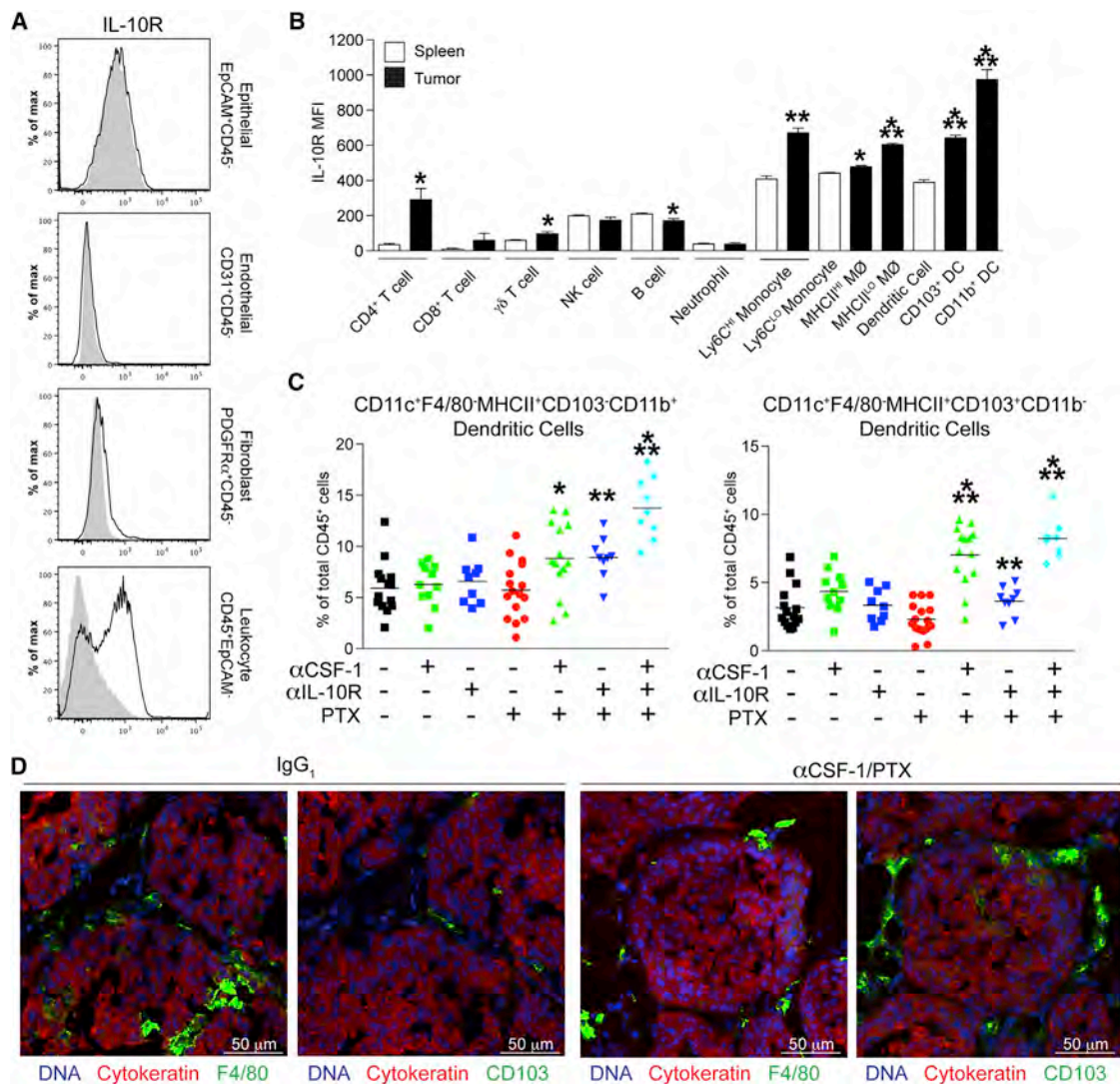


Figure 5. Expression of IL-10 Receptor by Tumor DCs

(A) Flow cytometric analysis of IL-10R surface expression for EpCAM⁺ epithelial cells, CD31⁺ endothelial cells, PDGFR α ⁺ fibroblasts, or CD45⁺ leukocytes in untreated MMTV-PyMT mice at end stage (>100 days). Fluorescence minus one (FMO) controls are shown in gray for each histogram. Representative data from one of three animals are shown.

(B) Surface expression of IL-10R measured by mean fluorescence intensity (MFI) minus background in various leukocyte populations from mammary tumors from MMTV-PyMT mice compared with similar populations in the spleens of non-tumor-bearing animals. Data are displayed as mean \pm SEM, with n = 3 mice per group. Significance was determined by an unpaired t test compared with the spleen, with *p < 0.05, **p < 0.01, and ***p < 0.001.

(C) Flow cytometric analysis of CD11c⁺F4/80⁺MHCII⁺CD103⁻CD11b⁺ DCs (left) or CD11c⁺F4/80⁺MHCII⁺CD103⁻CD11b⁻ DCs (right) in tumors from the MMTV-PyMT animals shown in Figure 2A. Significance was determined by an unpaired t test relative to IgG₁ or IgG₁/PTX control groups, with *p < 0.05, **p < 0.01, and ***p < 0.001.

(D) Localization of F4/80⁺ macrophages and CD103⁺ leukocytes within the tumor stroma of MMTV-PyMT tumors via immunofluorescent staining of serial sections. Representative images from one of three animals are displayed for both groups.

See also Figure S5.

(Figure 6A). Thus, although multiple leukocytes expressed *Il12a* mRNA, only DCs and macrophages appeared primed to produce IL-12. Indeed, IL-12p40 protein was only detectable by intracellular flow cytometry in a small population of tumor-associated CD103⁺ DCs (Figure 6B), the cell type expressing the highest levels of *Il12b* mRNA.

IL-10 regulates IL-12 production by macrophages and DCs in vitro, depending on the type and kinetics of stimulation (D'An-

drea et al., 1995; Koch et al., 1996). We thus affirmed that preincubation with IL-10 prevented IFN- γ /lipopolysaccharide (LPS)- and α CD40/LPS-induced production of IL-12p70 by FLT3-ligand matured bone marrow-derived DCs (BMDCs) (Figure 6C). This regulation occurred at the level of mRNA expression, as IL-10 prevented upregulation of *Il12a* mRNA following α CD40/LPS stimulation (Figure 6D) and upregulation of *Il12b* mRNA (Figure 6E) and the corresponding IL-12p40 protein

(Figure S6C) following stimulation by any combination of IFN- γ , LPS, or α CD40. Although IL-10 can induce downregulation of some Toll-like receptor (TLR) signaling components (Knödler et al., 2009), IL-10's capacity to suppress IL-12 expression was not dependent on suppressed DC activation, as CD86 expression was only mildly reduced by IL-10 during stimulation with IFN- γ / α CD40 or α CD40/LPS stimulation (Figure S6D).

Because these data indicated that IL-10 regulated IL-12 expression at the mRNA level in vitro, we isolated macrophages and DCs from mammary tumors 2 days following the second dose of PTX (day 7) to determine whether IL-10 was functionally regulating IL-12 expression in myeloid cells in vivo. Consistent with our previous findings (Figure S4), α IL-10R mAb/PTX therapy did not alter expression of either gene in isolated macrophages (Figure 6F). In both CD103⁻CD11b⁺ and CD103⁺CD11b⁻ DC populations, however, α IL-10R mAb/PTX therapy increased expression of *I12a*, with *I12b* expression also enhanced in CD103⁺CD11b⁻ DCs (Figure 6F). The upregulation of *I12b* and detection of IL-12p40 at the protein level in CD103⁺CD11b⁻ DCs indicates that these may be the critical source of IL-12 within mammary tumors; however, as IL-12p40 is produced in excess of IL-12p35, this is not definitive.

To evaluate whether IL-12 was functionally significant with regard to the enhanced CD8-dependent responses observed in either α IL-10R mAb/PTX or α CSF-1 mAb/PTX-treated experimental groups, late-stage MMTV-PyMT mice were treated with a neutralizing antibody against either IL-12p40 (recognizing IL-12 and IL-23) or IL-12p70 (recognizing only IL-12) prior to administration of PTX. Although neither α IL-12p40 mAb nor α IL-12p70 mAb altered the response of tumors to PTX alone (Figure 6G), both neutralizing mAbs blocked the improved response to PTX observed following α IL-10R mAb therapy (Figure 6G). Furthermore, consistent with our finding that macrophages were the primary source of IL-10 in mammary tumors (Figure 1), both IL-12 neutralizing antibodies also reversed the improved response to PTX observed following treatment with α CSF-1 mAb (Figure 6G).

IL12A Expression Correlates with Increased Pathologic Complete Response in Breast Cancer Patients

On the basis of these data indicating a significant role for IL-12 in mediating CD8⁺ T cells' responses to PTX in mammary carcinomas, we next evaluated whether *IL12A* or *IL12B* mRNA levels correlated with presence of DCs (Figure 7A) in human breast cancers using the TCGA data set (The Cancer Genome Atlas Network, 2012). Interestingly, only *IL12A* correlated with expression of transcription factors associated with DCs (*C/ITA*) or the human equivalent of the CD103⁺ DC subset (*BATF3*, *IRF8*). Expression of *IL12A*, but not *IL12B*, was also associated with evidence of a cytotoxic T cell response in these samples, as seen by a correlation with *GZMB*, *CD8A*, and *IFNG* expression (Figure 7B). On the basis of these associations, we next evaluated two published data sets annotated for pathologic complete response (pCR) following treatment with CTX (Hess et al., 2006; Tabchy et al., 2010). Here, high expression of *IL12A*, along with the DC transcription factors and cytotoxic effector molecules, all were associated with an improved rate of pCR, with an \sim 2-fold increase in the response rate observed for many of the genes (Figure 7C). Taken together, these results indicate an important

cytokine axis in breast cancers wherein macrophage-derived IL-10 suppresses IL-12 production by DCs during CTX, thereby limiting cytotoxic CD8⁺ T cell responses in carcinomas (Figure 8). Blockade of either the IL-10/IL-10R pathway or the CSF-1/CSF-1R pathway thus improves response to CTX and increases survival of tumor-bearing mice.

DISCUSSION

Herein we describe an interaction between macrophages and DCs in mammary tumor microenvironments, wherein macrophage-derived IL-10 indirectly blunts CD8⁺ T cell responses by inhibiting DC production of IL-12 following CTX. Tumor-associated macrophages have long been described to possess an immunosuppressive phenotype (Mantovani et al., 2002), but the in vivo relevance of this phenotype has largely been inferred. Direct suppression by immature myeloid cells is usually linked to metabolism of L-arginine or production of free radicals (Gabrilovich and Nagaraj, 2009). Supporting a role for these pathways in macrophage-mediated suppression, hypoxia promotes macrophage suppressive capacity and induces expression of arginase-1 (Doedens et al., 2010), macrophages can suppress T cell proliferation through L-arginine depletion (Rodriguez et al., 2003), and, as reported herein, MHCII^{LO} macrophages exhibit tropism for hypoxic regions and exhibit enhanced suppressive capacity. However, the degree to which nutrient depletion in a closed in vitro system reflects the tumor microenvironment is unclear, and other studies have found that MHCII^{LO} macrophages from implanted lung carcinoma models (Movahedi et al., 2010) and macrophages from human ovarian carcinoma ascites (Kryczek et al., 2006) suppress T cell proliferation independent of arginase and nitric oxide synthase activity. Human macrophages have instead been found to directly suppress T cell responses through programmed death-ligand 1 in hepatocellular carcinoma (Kuang et al., 2009) and B7-H4 in ovarian carcinoma (Kryczek et al., 2006), and possibly indirectly through T_{Reg} cell recruitment through CCL22 (Curiel et al., 2004). Along with these studies, data presented herein describe a functional role for macrophages in mediating immune suppression within tumors, and ascribe this role to suppression of DC function.

The drivers of *I10* expression by tumor macrophages are unclear. In general, *I10* expression by macrophages is thought to reflect activation by TLR ligands and type I IFN (Saraiva and O'Garra, 2010). We noted modestly elevated expression of *I10* from MHCII^{LO} macrophages, but although higher IL-10 secretion has also been observed in MHCII^{LO} macrophages from implanted lung carcinomas (Laoui et al., 2014), there is no evidence that hypoxia promotes *I10* expression. MHCII^{LO} macrophages also expressed higher surface levels of IL-4R α , but we previously reported that absence of CD4⁺ T cells did not influence IL-10 production by macrophages despite the ability of both IL-4 and IL-13 to promote IL-10 production in vitro (DeNardo et al., 2009). Notably, mammary gland macrophages constitutively expressed *I10* at levels equivalent to that found in tumor macrophages, indicating that the homeostatic environment of the mammary gland is sufficient to promote *I10* expression, without a requirement for properties of the tumor microenvironment such as inflammation or hypoxia.

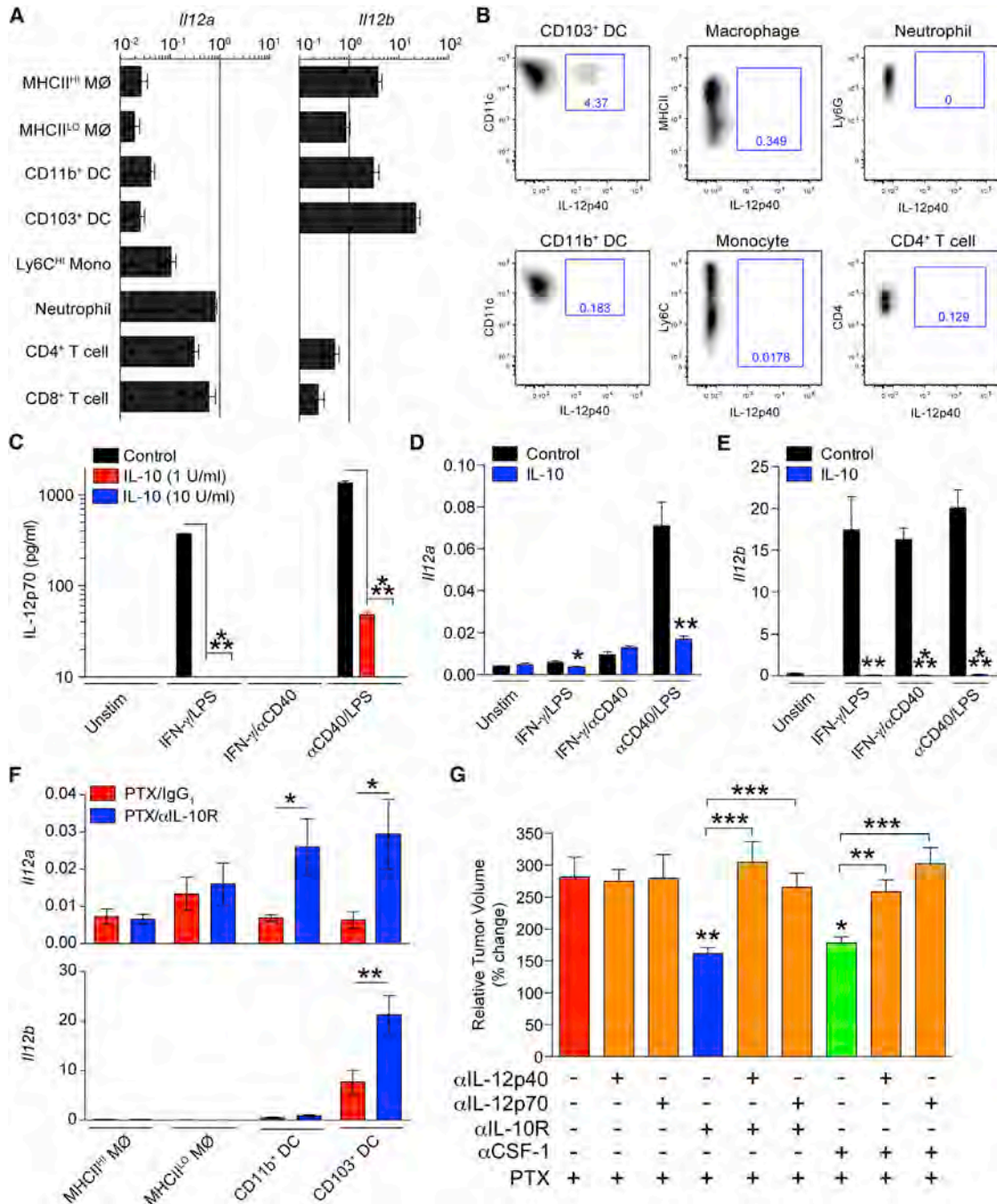


Figure 6. Response to PTX Is Dependent on IL-12 Expression by DCs

(A) *Il12a* or *Il12b* mRNA expression levels in fluorescence-activated cell-sorted leukocytes from mammary tumors of MMTV-PyMT mice as determined by real-time PCR. Data are normalized to *Tbp* expression and displayed as mean \pm SEM, with n = 8 per cell type.

(B) Detection of IL-12p40 by intracellular flow cytometry in tumor leukocytes following in vivo administration of brefeldin A. Representative data from one of two animals are shown.

(C) Production of IL-12p70 by BMDCs as measured by ELISA following 24 hr stimulation with IFN- γ /LPS, IFN- γ / α CD40, or α CD40/LPS. Cells were pretreated for 24 hr with 1 or 10 U/ml of IL-10 prior to stimulation.

(D and E) Expression of *Il12a* (D) or *Il12b* (E) mRNA by BMDCs as measured by RT-PCR. Cells were pretreated for 24 hr with 10 U/ml of IL-10 prior to stimulation. For (C) to (E), data are displayed as mean \pm SEM, samples were assayed in quadruplicate, and one of two representative experiments is shown. Significance was determined by an unpaired t test relative to the control group, with *p < 0.05, **p < 0.01, and ***p < 0.001.

(F) *Il12a* or *Il12b* mRNA expression levels in fluorescence-activated cell-sorted MØ and DC populations from mammary tumors of MMTV-PyMT mice 2 days following the second dose of PTX (day 7) in combination with α IL-10R mAb. Data are normalized to *Tbp* expression and displayed as mean \pm SEM, with n \geq 4 mice per cell type. Significance determined by a Mann-Whitney test, with *p < 0.05 and **p < 0.01.

(legend continued on next page)

IL-10 has the potential to be expressed by most leukocyte populations (Saraiva and O'Garra, 2010), as well as by normal and malignant epithelial cells (O'Garra et al., 2008). Despite this extensive expression capacity, IL-10 production specifically by T_{Reg} cells is critical for maintaining tolerance in the colon (Saraiva and O'Garra, 2010), limiting T_H17 inflammation in tumors (Stewart et al., 2013), and suppressing polyp formation (Dennis et al., 2013). In contrast to the colon, we found that in mammary carcinomas, macrophages expressed the highest level of *Il10* mRNA, with 10-fold lower expression observed in other leukocytes, and no expression observed by tumor epithelia. As the dominant immune population in murine mammary tumors, macrophages are thus the critical source of IL-10.

In human breast cancer, we similarly found no association between *FOXP3* and *IL10* expression but rather observed a correlation between *IL10* expression and genes associated with either the presence (*CSF1R*, *CD14*, *CD68*) or polarization (*CD163*, *MSR1*) of macrophages. With no evidence of toxicity and the potential to simultaneously block multiple pro-tumorigenic macrophage pathways, targeting of the CSF-1/CSF-1R pathway continues to be an attractive therapeutic approach. That said, the increased diversity of leukocytic infiltrates in human breast cancer (Ruffell et al., 2012b), and our observation that breast tumor epithelial cells expressed IL-10, argues that neutralizing the effects of IL-10 in human breast cancer may require more selective targeting to maximize a cytotoxic T cell response during CTX. This could take the form of a human α IL-10R blocking antibody, or kinase inhibitors against downstream IL-10R signaling components such as Janus kinase 1 or Signal transducer and activator of transcription 3. It might also be possible to enhance chemotherapeutic efficacy by directly activating myeloid cells to produce increased levels of IL-12, either alone or in combination with IL-10R antagonists. Although toxicity resulting from systemic myeloid activation is a concern, it is promising to note that a relatively safe CD40 agonist is in clinical trials (Beatty et al., 2013).

IL-10 is often referred to as a pleiotropic cytokine, and its dual role in cancer likely reflects this. Both IL-10 deficiency and IL-10 overexpression can promote antitumor immune responses in mice (O'Garra et al., 2008). Although IL-10-deficient mice are resistant to ultraviolet-induced skin carcinogenesis (Loser et al., 2007), they are also sensitive to skin and colon carcinogenesis (Mumm et al., 2011; Sturlan et al., 2001). Some of this disparity most assuredly reflects the significance of local tumor microenvironments in sculpting immune responses but also likely reflects local variations in bioavailable IL-10 (O'Garra et al., 2008). IL-10 is a potent suppressor of DC activation, with even 1.0 U/ml largely ablating IL-12 secretion, as well as suppressing DC differentiation in vitro (Allavena et al., 1998). On the other hand, high concentrations of IL-10 can promote IL-2-dependent proliferation of CD8⁺ T cells (Chen and Zlotnik, 1991; Groux et al., 1998), and IL-10 is involved in CD8⁺ T cell memory formation in some, but not all, infection models (O'Garra

et al., 2008). This has led to divergent approaches for targeting IL-10 as an anticancer therapeutic: blocking IL-10R to enhance myeloid cell function (Vicari et al., 2002) versus injecting exogenous IL-10 to directly promote an antitumor T cell response through activation of intratumoral CD8⁺ T cells (Emmerich et al., 2012; Mumm et al., 2011). CD8⁺ T cells in mammary tumors of MMTV-PyMT did not express IL-10R, indicating that exogenous IL-10 would likely prove ineffective in this context, but ongoing clinical studies will determine the validity of this approach in patients.

Blocking IL-10R has not been used extensively as an approach for anticancer therapy but has been reported to induce tumor regression in combination with CpG oligonucleotides in various subcutaneous tumor models, ostensibly through macrophage/DC activation and increased expression of IL-12 (Guiducci et al., 2005; Vicari et al., 2002). In sharp contrast to these studies, response to CTX in subcutaneous tumor models has been found to occur independently of IL-12 and *Batf3*-dependent DCs and is instead mediated by an immune cell/cytokine pathway involving IFN- β , IL-17, and IFN- γ , with production by CD11b⁺CD103⁺ DCs, $\gamma\delta$ T cells, and CD8⁺ T cells, respectively (Kroemer et al., 2013; Ma et al., 2013). The importance of this pathway for response to CTX has been called into question using transgenic models of mammary carcinoma, as these respond to CTX independently of adaptive immune cells, with the suggestion that this is due to the use of implantable versus spontaneous tumors (Ciampricotti et al., 2012). We instead suggest that these differences are due at least partially to anatomical location. Thus, preventing macrophage infiltration via α CSF-1 mAbs (or CSF-1R antagonists) or limiting macrophage functionality via α IL-10R mAbs, enables CTX and resultant cell death to benefit from productive CD8⁺ T cell responses elicited in tumors. However, unlike subcutaneous models, our data indicate a critical role for IL-12 and possibly CD103⁺ DCs, again highlighting the role of anatomical location in determining response to therapy. This concept has been elegantly demonstrated in a recent study in which subcutaneously implanted tumors were found to be more sensitive to immunotherapy than the same cell lines implanted orthotopically (Devaud et al., 2014).

DCs in solid tumors are generally viewed as critical primers of de novo T cell responses (Chen and Mellman, 2013), and therapeutic targeting of DCs has focused on this aspect. Our data do not definitively demonstrate a role for DCs within mammary tumors, and systemic suppression of DC function through IL-10 has been observed (Yang and Lattime, 2003). At the same time, however, removal of tumor-draining lymph nodes from mice bearing subcutaneous tumors did not alter response to CTX (Ma et al., 2013), tertiary lymphoid structures have been implicated in T cell activity in melanoma (Chen et al., 2013), and the presence of follicular helper T cells correlates positively with patient outcome and response to CTX in breast cancer (Bindea et al., 2013; Gu-Trantien et al., 2013). These studies align well with our finding that gene expression indicative of a CD8⁺

(G) Relative tumor volume after 3 rounds of PTX in MMTV-PyMT transgenic mice following combination therapy with α CSF-1 mAb or α IL-10R mAb. IL-12 neutralizing mAb (α IL-12p40 or α IL-12p70) was administered concurrently every 5 days. Data are displayed as mean \pm SEM, with $n \geq 5$ mice per group. Significance was determined by an unpaired t test, with * $p < 0.05$, ** $p < 0.01$, and *** $p < 0.001$. See also Figure S6.

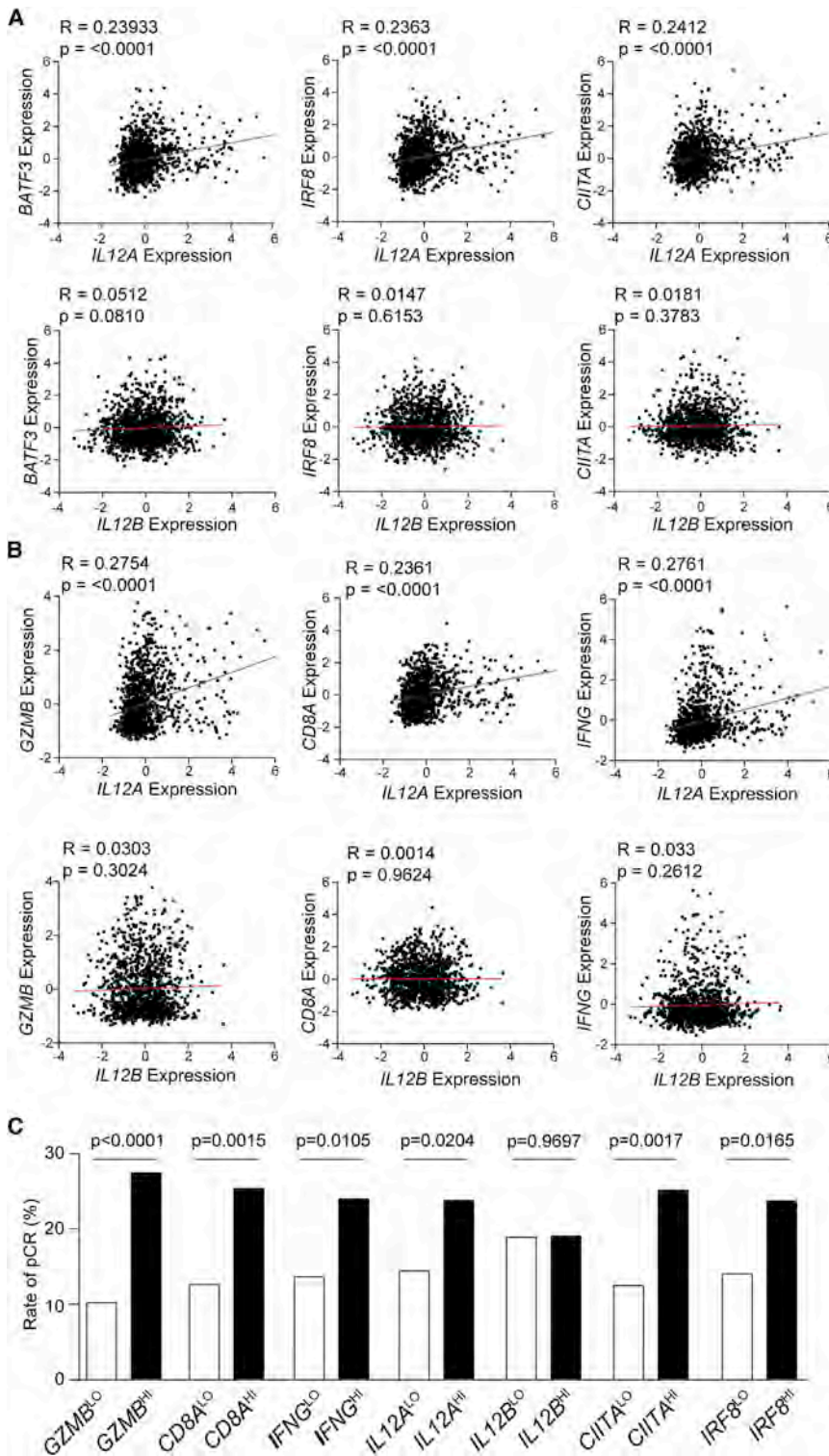


Figure 7. IL12A Expression Correlates with pCR Rates in Breast Cancer

(A) Linear regression analysis between *IL12A* or *IL12B* expression and various DC-associated genes (*CCR7*, *IRF8*, and *CIITA*) in human breast cancer samples from the TCGA data set (n = 1,161).

(B) Linear regression analysis between *IL12A* or *IL12B* expression and various cytotoxic lymphocyte-associated genes (*GZMB*, *CD8A*, and *IFNG*) in human breast cancer samples from the TCGA data set.

(C) Frequency of pCR in patients separated by median expression for genes associated with a cytotoxic T cell response (*GZMB*, *CD8A*, and *IFNG*) or DCs (*IL12A*, *CIITA*, *CCR7*, and *IRF8*). Data reflect a cohort of 379 patients constructed from two independent data sets. Significance was determined by a chi-square test.

EXPERIMENTAL PROCEDURES

Ethics Statement

Deidentified human tissue was received from the University of California, San Francisco (UCSF), Department of Pathology, with patient consent forms obtained at the time of tissue acquisition. Authorization for the use of samples was through the UCSF Committee on Human Research (05028310) under "exempt category 4" for individuals receiving deidentified biological specimens.

Animal Care and Use

FVB/n strain background mice harboring the PyMT transgene under the control of the MMTV promoter (Guy et al., 1992), and the simian virus 40 large tumor antigen (SV40 TAG) under control of the rat prostatic steroid binding protein gene [C3(1)] (Maroulakou et al., 1994), have been previously described. Implantation of orthotopic mammary tumors was performed as described (DeNardo et al., 2011) using single-cell suspensions from mammary tumors of d80-d85 MMTV-PyMT transgenic mice combined 1:1 with Matrigel (BD Biosciences). Treatment schedules were initiated as indicated in the respective figures. mAbs (α CSF-1/5A1, α IL-10R/1B1.3A, α CD8/2.43, IgG₁/HRPN, α IL-12p75/R2-9A5, and α IL-12p40/C17.8) were obtained from BioXCell and were administered by intraperitoneal injection at 1.0 mg/mouse, with follow-up doses of 0.5 mg every 5 days. Clinical grade PTX (Hospira) or carboplatin (Novapilus) was administered intravenously every 5 days at 10 mg/kg or 50 mg/kg, respectively. Before terminal cardiac perfusion with PBS containing 10 U/ml of heparin (Sigma-Aldrich), mice were intraperitoneally injected with 50 mg/kg BrdU (Roche) for 90 min. Resected tissues were either flash frozen in liquid nitrogen, directly embedded in optimal cutting temperature (Sakura Finetek) medium after

T cell response (*GZMB*, *CD8A*, *IFNG*) or the presence of DCs (*IL12A*, *CIITA*, *IRF8*) coincides with improved response to neoadjuvant CTX, and together hint at the importance of favorable DC activity within the tumor microenvironment promoting an anti-tumor immune response to CTX.

resection, or incubated overnight in neutral buffered formalin prior to ethanol dehydration and paraffin embedding. Mice were maintained either within the UCSF Laboratory for Animal Care barrier facility or the Oregon Health & Science University Department of Comparative Medicine barrier facility. All experiments involving animals were approved by the respective institutional animal care and use committees.

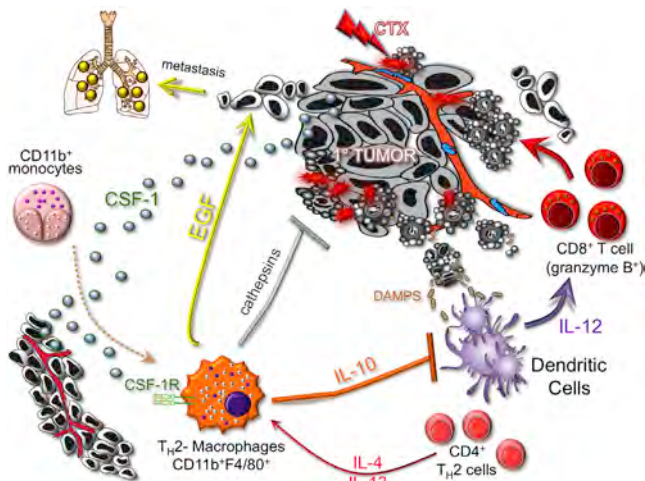


Figure 8. Model of IL-10 Suppressing IL-12 Production by Dendritic Cells and Limiting the CD8⁺ T Cell-Dependent Response to CTX in Mammary Carcinomas

CD11b⁺ monocytes are recruited into mammary tumors through increased CSF-1 gradients largely derived from epithelial cells. Once in tissue or tumor parenchyma, differentiated macrophages stimulate invasion and metastasis through EGF, which is induced in response to CSF-1, in combination with IL-4/IL-13 derived from CD4⁺ T cells. IL-4/IL-13 also induces expression and/or activity of cathepsin proteases, directly promoting resistance to CTX-induced cell death. Macrophages further suppress CTX efficacy by indirectly limiting a cytotoxic T cell response. Macrophage-derived IL-10 suppresses the ability of DCs to produce IL-12 during CTX, likely in response to damage-associated molecular patterns (DAMPs). In the absence of macrophages or IL-10, IL-12 is able to promote a productive CD8⁺ T cell response, thereby enhancing the efficacy of CTX.

Statistical Analysis

Statistical analyses were performed using Prism (GraphPad). Statistical significance was determined via an unpaired t test, an unpaired t test with Welch's correction, 2-way analysis of variance (ANOVA), or Mann-Whitney test as indicated. Heatmaps were generated GENE-E software (<http://www.broadinstitute.org/cancer/software/GENE-E/>). All heatmaps are displayed on a logarithmic scale with values normalized per row, with hierarchical clustering performed with a 1 minus Pearson correlation. Linear regression analysis in breast cancer was performed in Prism using the TCGA data set ([The Cancer Genome Atlas Network, 2012](http://www.cancer.gov/genome-atlas-network)). Gene expression data from fine-needle aspirate obtained prior to neoadjuvant CTX in breast cancer patients were obtained from 2 published data sets (GSE20194 and GSE20271) annotated for pCR (Hess et al., 2006; Tabchy et al., 2010).

SUPPLEMENTAL INFORMATION

Supplemental Information includes Supplemental Experimental Procedures and six figures and can be found with this article online at <http://dx.doi.org/10.1016/j.ccell.2014.09.006>.

ACKNOWLEDGMENTS

We thank Heather I. Chen, Alexander Forsyth, Paul Huynh, and Anna Shvygina for technical assistance; Anna Wasiuk and Tina Bose for helpful discussion; Nesrine I. Affara for graphics; and support from the Knight Cancer Center Flow Cytometry, Bioinformatics, and Advanced Light Microscopy shared resources. We acknowledge support from the Department of Defense Breast Cancer Research Program (W81XWH-09-1-0543) and a Knight Cancer Institute Career Development Award to B.R. Research reported herein was supported by the National Cancer Institute of the NIH (grants R01CA130980,

R01CA140943, R01CA15531, and U54CA163123), the Department of Defense Breast Cancer Research Program (grant W81XWH-11-1-0702), the Susan G. Komen Foundation (grants KG110560 and KG111084), and the Breast Cancer Research Foundation. D.C.-S., V.C., N.P., and D.D. are/were employees of Novartis International, AG.

Received: July 14, 2014

Revised: September 7, 2014

Accepted: September 15, 2014

Published: October 16, 2014

REFERENCES

- Allavena, P., Piemonti, L., Longoni, D., Bernasconi, S., Stoppacciaro, A., Ruco, L., and Mantovani, A. (1998). IL-10 prevents the differentiation of monocytes to dendritic cells but promotes their maturation to macrophages. *Eur. J. Immunol.* **28**, 359–369.
- Beatty, G.L., Torigian, D.A., Chiorean, E.G., Saboury, B., Brothers, A., Alavi, A., Troxel, A.B., Sun, W., Teitelbaum, U.R., Vonderheide, R.H., and O'Dwyer, P.J. (2013). A phase I study of an agonist CD40 monoclonal antibody (CP-870,893) in combination with gemcitabine in patients with advanced pancreatic ductal adenocarcinoma. *Clin. Cancer Res.* **19**, 6286–6295.
- Bindea, G., Mlecnik, B., Tosolini, M., Kirilovsky, A., Waldner, M., Obenauf, A.C., Angell, H., Fredriksen, T., Lafontaine, L., Berger, A., et al. (2013). Spatiotemporal dynamics of intratumoral immune cells reveal the immune landscape in human cancer. *Immunity* **39**, 782–795.
- Bingle, L., Brown, N.J., and Lewis, C.E. (2002). The role of tumour-associated macrophages in tumour progression: implications for new anticancer therapies. *J. Pathol.* **196**, 254–265.
- Chen, D.S., and Mellman, I. (2013). Oncology meets immunology: the cancer-immunity cycle. *Immunity* **39**, 1–10.
- Chen, W.F., and Zlotnik, A. (1991). IL-10: a novel cytotoxic T cell differentiation factor. *J. Immunol.* **147**, 528–534.
- Chen, L., Fabian, K.L., Taylor, J.L., and Storkus, W.J. (2013). Therapeutic use of dendritic cells to promote the extranodal priming of anti-tumor immunity. *Front. Immunol.* **4**, 388.
- Ciampricotti, M., Hau, C.S., Doornebal, C.W., Jonkers, J., and de Visser, K.E. (2012). Chemotherapy response of spontaneous mammary tumors is independent of the adaptive immune system. *Nat. Med.* **18**, 344–346, author reply 346.
- Curiel, T.J., Coukos, G., Zou, L., Alvarez, X., Cheng, P., Mottram, P., Evdemon-Hogan, M., Conejo-Garcia, J.R., Zhang, L., Burow, M., et al. (2004). Specific recruitment of regulatory T cells in ovarian carcinoma fosters immune privilege and predicts reduced survival. *Nat. Med.* **10**, 942–949.
- D'Andrea, A., Ma, X., Aste-Amezaga, M., Paganin, C., and Trinchieri, G. (1995). Stimulatory and inhibitory effects of interleukin (IL)-4 and IL-13 on the production of cytokines by human peripheral blood mononuclear cells: priming for IL-12 and tumor necrosis factor alpha production. *J. Exp. Med.* **181**, 537–546.
- Deeb, K.K., Michalowska, A.M., Yoon, C.Y., Krummey, S.M., Hoenerhoff, M.J., Kavanaugh, C., Li, M.C., Demayo, F.J., Linnoila, I., Deng, C.X., et al. (2007). Identification of an integrated SV40 T/t-antigen cancer signature in aggressive human breast, prostate, and lung carcinomas with poor prognosis. *Cancer Res.* **67**, 8065–8080.
- DeNardo, D.G., Barreto, J.B., Andreu, P., Vasquez, L., Tawfik, D., Kolhatkar, N., and Coussens, L.M. (2009). CD4(+) T cells regulate pulmonary metastasis of mammary carcinomas by enhancing protumor properties of macrophages. *Cancer Cell* **16**, 91–102.
- DeNardo, D.G., Brennan, D.J., Rexhepaj, E., Ruffell, B., Shiao, S.L., Madden, S.F., Gallagher, W.M., Wadhvani, N., Keil, S.D., Junaid, S.A., et al. (2011). Leukocyte complexity predicts breast cancer survival and functionally regulates response to chemotherapy. *Cancer Discov* **1**, 54–67.
- Denning, T.L., Campbell, N.A., Song, F., Garofalo, R.P., Klimpel, G.R., Reyes, V.E., and Ernst, P.B. (2000). Expression of IL-10 receptors on epithelial cells from the murine small and large intestine. *Int. Immunol.* **12**, 133–139.
- Dennis, K.L., Wang, Y., Blatner, N.R., Wang, S., Saadalla, A., Trudeau, E., Roers, A., Weaver, C.T., Lee, J.J., Gilbert, J.A., et al. (2013). Adenomatous

- polyps are driven by microbe-instigated focal inflammation and are controlled by IL-10-producing T cells. *Cancer Res.* 73, 5905–5913.
- Devaud, C., Westwood, J.A., John, L.B., Flynn, J.K., Paquet-Fiffeld, S., Duong, C.P., Yong, C.S., Pegram, H.J., Stacker, S.A., Achen, M.G., et al. (2014). Tissues in different anatomical sites can sculpt and vary the tumor microenvironment to affect responses to therapy. *Mol. Ther.* 22, 18–27.
- Doedens, A.L., Stockmann, C., Rubinstein, M.P., Liao, D., Zhang, N., DeNardo, D.G., Coussens, L.M., Karin, M., Goldrath, A.W., and Johnson, R.S. (2010). Macrophage expression of hypoxia-inducible factor-1 alpha suppresses T-cell function and promotes tumor progression. *Cancer Res.* 70, 7465–7475.
- Emmerich, J., Mumm, J.B., Chan, I.H., LaFace, D., Truong, H., McClanahan, T., Gorman, D.M., and Oft, M. (2012). IL-10 directly activates and expands tumor-resident CD8(+) T cells without de novo infiltration from secondary lymphoid organs. *Cancer Res.* 72, 3570–3581.
- Gabrilovich, D.I., and Nagaraj, S. (2009). Myeloid-derived suppressor cells as regulators of the immune system. *Nat. Rev. Immunol.* 9, 162–174.
- Groux, H., Bigler, M., de Vries, J.E., and Roncarolo, M.G. (1998). Inhibitory and stimulatory effects of IL-10 on human CD8+ T cells. *J. Immunol.* 160, 3188–3193.
- Gu-Trantien, C., Loi, S., Garaud, S., Equeter, C., Libin, M., de Wind, A., Ravoet, M., Le Buanec, H., Sibille, C., Manfouo-Foutsop, G., et al. (2013). CD4+ follicular helper T cell infiltration predicts breast cancer survival. *J. Clin. Invest.* 123, 2873–2892.
- Guiducci, C., Vicari, A.P., Sangaletti, S., Trinchieri, G., and Colombo, M.P. (2005). Redirecting in vivo elicited tumor infiltrating macrophages and dendritic cells towards tumor rejection. *Cancer Res.* 65, 3437–3446.
- Guy, C.T., Cardiff, R.D., and Muller, W.J. (1992). Induction of mammary tumors by expression of polyomavirus middle T oncogene: a transgenic mouse model for metastatic disease. *Mol. Cell. Biol.* 12, 954–961.
- Hess, K.R., Anderson, K., Symms, W.F., Valero, V., Ibrahim, N., Mejia, J.A., Booser, D., Theriault, R.L., Buzdar, A.U., Dempsey, P.J., et al. (2006). Pharmacogenomic predictor of sensitivity to preoperative chemotherapy with paclitaxel and fluorouracil, doxorubicin, and cyclophosphamide in breast cancer. *J. Clin. Oncol.* 24, 4236–4244.
- Knödler, A., Schmidt, S.M., Bringmann, A., Weck, M.M., Brauer, K.M., Holderried, T.A., Heine, A.K., Grünebach, F., and Brossart, P. (2009). Post-transcriptional regulation of adapter molecules by IL-10 inhibits TLR-mediated activation of antigen-presenting cells. *Leukemia* 23, 535–544.
- Koch, F., Stanzl, U., Jennewein, P., Janke, K., Heufler, C., Kämpgen, E., Romani, N., and Schuler, G. (1996). High level IL-12 production by murine dendritic cells: upregulation via MHC class II and CD40 molecules and downregulation by IL-4 and IL-10. *J. Exp. Med.* 184, 741–746.
- Kroemer, G., Galluzzi, L., Kepp, O., and Zitvogel, L. (2013). Immunogenic cell death in cancer therapy. *Annu. Rev. Immunol.* 31, 51–72.
- Kryczek, I., Zou, L., Rodriguez, P., Zhu, G., Wei, S., Mottram, P., Brumlik, M., Cheng, P., Curiel, T., Myers, L., et al. (2006). B7-H4 expression identifies a novel suppressive macrophage population in human ovarian carcinoma. *J. Exp. Med.* 203, 871–881.
- Kuang, D.M., Zhao, Q., Peng, C., Xu, J., Zhang, J.P., Wu, C., and Zheng, L. (2009). Activated monocytes in peritumoral stroma of hepatocellular carcinoma foster immune privilege and disease progression through PD-L1. *J. Exp. Med.* 206, 1327–1337.
- Laoui, D., Van Overmeire, E., Di Conza, G., Aldeni, C., Keirse, J., Morias, Y., Movahedi, K., Houbracken, I., Schouppe, E., Elkrim, Y., et al. (2014). Tumor hypoxia does not drive differentiation of tumor-associated macrophages but rather fine-tunes the M2-like macrophage population. *Cancer Res.* 74, 24–30.
- Lin, E.Y., Nguyen, A.V., Russell, R.G., and Pollard, J.W. (2001). Colony-stimulating factor 1 promotes progression of mammary tumors to malignancy. *J. Exp. Med.* 193, 727–740.
- Loser, K., Apelt, J., Voskort, M., Mohaupt, M., Balkow, S., Schwarz, T., Grabbe, S., and Beissert, S. (2007). IL-10 controls ultraviolet-induced carcinogenesis in mice. *J. Immunol.* 179, 365–371.
- Ma, Y., Adjemian, S., Mattarollo, S.R., Yamazaki, T., Aymeric, L., Yang, H., Portela Catani, J.P., Hannani, D., Duret, H., Steegh, K., et al. (2013). Anticancer chemotherapy-induced intratumoral recruitment and differentiation of antigen-presenting cells. *Immunity* 38, 729–741.
- Mantovani, A., Sozzani, S., Locati, M., Allavena, P., and Sica, A. (2002). Macrophage polarization: tumor-associated macrophages as a paradigm for polarized M2 mononuclear phagocytes. *Trends Immunol.* 23, 549–555.
- Maroulakou, I.G., Anver, M., Garrett, L., and Green, J.E. (1994). Prostate and mammary adenocarcinoma in transgenic mice carrying a rat C3(1) simian virus 40 large tumor antigen fusion gene. *Proc. Natl. Acad. Sci. U S A* 91, 11236–11240.
- Mok, S., Koya, R.C., Tsui, C., Xu, J., Robert, L., Wu, L., Graeber, T.G., West, B.L., Bollag, G., and Ribas, A. (2014). Inhibition of CSF-1 receptor improves the antitumor efficacy of adoptive cell transfer immunotherapy. *Cancer Res.* 74, 153–161.
- Moore, K.W., de Waal Malefyt, R., Coffman, R.L., and O'Garra, A. (2001). Interleukin-10 and the interleukin-10 receptor. *Annu. Rev. Immunol.* 19, 683–765.
- Movahedi, K., Laoui, D., Gysemans, C., Baeten, M., Stangé, G., Van den Bossche, J., Mack, M., Pipeleers, D., In't Veld, P., De Baetselier, P., and Van Ginderachter, J.A. (2010). Different tumor microenvironments contain functionally distinct subsets of macrophages derived from Ly6C(high) monocytes. *Cancer Res.* 70, 5728–5739.
- Mumm, J.B., Emmerich, J., Zhang, X., Chan, I., Wu, L., Mauze, S., Blaisdell, S., Basham, B., Dai, J., Grein, J., et al. (2011). IL-10 elicits IFN γ -dependent tumor immune surveillance. *Cancer Cell* 20, 781–796.
- O'Garra, A., Barrat, F.J., Castro, A.G., Vicari, A., and Hawrylowicz, C. (2008). Strategies for use of IL-10 or its antagonists in human disease. *Immunol. Rev.* 223, 114–131.
- Pollard, J.W. (2009). Trophic macrophages in development and disease. *Nat. Rev. Immunol.* 9, 259–270.
- Pyonteck, S.M., Akkari, L., Schuhmacher, A.J., Bowman, R.L., Sevenich, L., Quail, D.F., Olson, O.C., Quick, M.L., Huse, J.T., Teijeiro, V., et al. (2013). CSF-1R inhibition alters macrophage polarization and blocks glioma progression. *Nat. Med.* 19, 1264–1272.
- Radi, Z.A., Koza-Taylor, P.H., Bell, R.R., Obert, L.A., Runnels, H.A., Beebe, J.S., Lawton, M.P., and Sadis, S. (2011). Increased serum enzyme levels associated with kupffer cell reduction with no signs of hepatic or skeletal muscle injury. *Am. J. Pathol.* 179, 240–247.
- Ries, C.H., Cannarile, M.A., Hoves, S., Benz, J., Wartha, K., Runza, V., Rey-Giraud, F., Pradel, L.P., Feuerhake, F., Klamann, I., et al. (2014). Targeting tumor-associated macrophages with anti-CSF-1R antibody reveals a strategy for cancer therapy. *Cancer Cell* 25, 846–859.
- Rodriguez, P.C., Zea, A.H., DeSalvo, J., Culotta, K.S., Zabaleta, J., Quiceno, D.G., Ochoa, J.B., and Ochoa, A.C. (2003). L-arginine consumption by macrophages modulates the expression of CD3 zeta chain in T lymphocytes. *J. Immunol.* 171, 1232–1239.
- Ruffell, B., Affara, N.I., and Coussens, L.M. (2012a). Differential macrophage programming in the tumor microenvironment. *Trends Immunol.* 33, 119–126.
- Ruffell, B., Au, A., Rugo, H.S., Esserman, L.J., Hwang, E.S., and Coussens, L.M. (2012b). Leukocyte composition of human breast cancer. *Proc. Natl. Acad. Sci. U S A* 109, 2796–2801.
- Saraiva, M., and O'Garra, A. (2010). The regulation of IL-10 production by immune cells. *Nat. Rev. Immunol.* 10, 170–181.
- Shree, T., Olson, O.C., Elie, B.T., Kester, J.C., Garfall, A.L., Simpson, K., Bell-McGuinn, K.M., Zabor, E.C., Brogi, E., and Joyce, J.A. (2011). Macrophages and cathepsin proteases blunt chemotherapeutic response in breast cancer. *Genes Dev.* 25, 2465–2479.
- Stewart, C.A., Metheny, H., Iida, N., Smith, L., Hanson, M., Steinhagen, F., Leighty, R.M., Roers, A., Karp, C.L., Müller, W., and Trinchieri, G. (2013). Interferon-dependent IL-10 production by Tregs limits tumor Th17 inflammation. *J. Clin. Invest.* 123, 4859–4874.
- Stockmann, C., Doedens, A., Weidemann, A., Zhang, N., Takeda, N., Greenberg, J.I., Cheresch, D.A., and Johnson, R.S. (2008). Deletion of vascular

endothelial growth factor in myeloid cells accelerates tumorigenesis. *Nature* 456, 814–818.

Strachan, D.C., Ruffell, B., Oei, Y., Bissell, M.J., Coussens, L.M., Pryer, N., and Daniel, D. (2013). CSF1R inhibition delays cervical and mammary tumor growth in murine models by attenuating the turnover of tumor-associated macrophages and enhancing infiltration by CD8(+) T cells. *Oncolmmunology* 2, e26968.

Sturlan, S., Oberhuber, G., Beinhauer, B.G., Tichy, B., Kappel, S., Wang, J., and Rogy, M.A. (2001). Interleukin-10-deficient mice and inflammatory bowel disease associated cancer development. *Carcinogenesis* 22, 665–671.

Tabchy, A., Valero, V., Vidaurre, T., Lluch, A., Gomez, H., Martin, M., Qi, Y., Barajas-Figueroa, L.J., Souchon, E., Coutant, C., et al. (2010). Evaluation of a 30-gene paclitaxel, fluorouracil, doxorubicin, and cyclophosphamide chemotherapy response predictor in a multicenter randomized trial in breast cancer. *Clin. Cancer Res.* 16, 5351–5361.

The Cancer Genome Atlas Network (2012). Comprehensive molecular portraits of human breast tumours. *Nature* 490, 61–70.

Trinchieri, G. (2003). Interleukin-12 and the regulation of innate resistance and adaptive immunity. *Nat. Rev. Immunol.* 3, 133–146.

Vicari, A.P., Chiodoni, C., Vaure, C., Ait-Yahia, S., Dercamp, C., Matsos, F., Reynard, O., Taverne, C., Merle, P., Colombo, M.P., et al. (2002). Reversal of tumor-induced dendritic cell paralysis by CpG immunostimulatory oligonucleotide and anti-interleukin 10 receptor antibody. *J. Exp. Med.* 196, 541–549.

Wei, S., Lightwood, D., Ladyman, H., Cross, S., Neale, H., Griffiths, M., Adams, R., Marshall, D., Lawson, A., McKnight, A.J., and Stanley, E.R. (2005). Modulation of CSF-1-regulated post-natal development with anti-CSF-1 antibody. *Immunobiology* 210, 109–119.

Yang, A.S., and Lattime, E.C. (2003). Tumor-induced interleukin 10 suppresses the ability of splenic dendritic cells to stimulate CD4 and CD8 T-cell responses. *Cancer Res.* 63, 2150–2157.

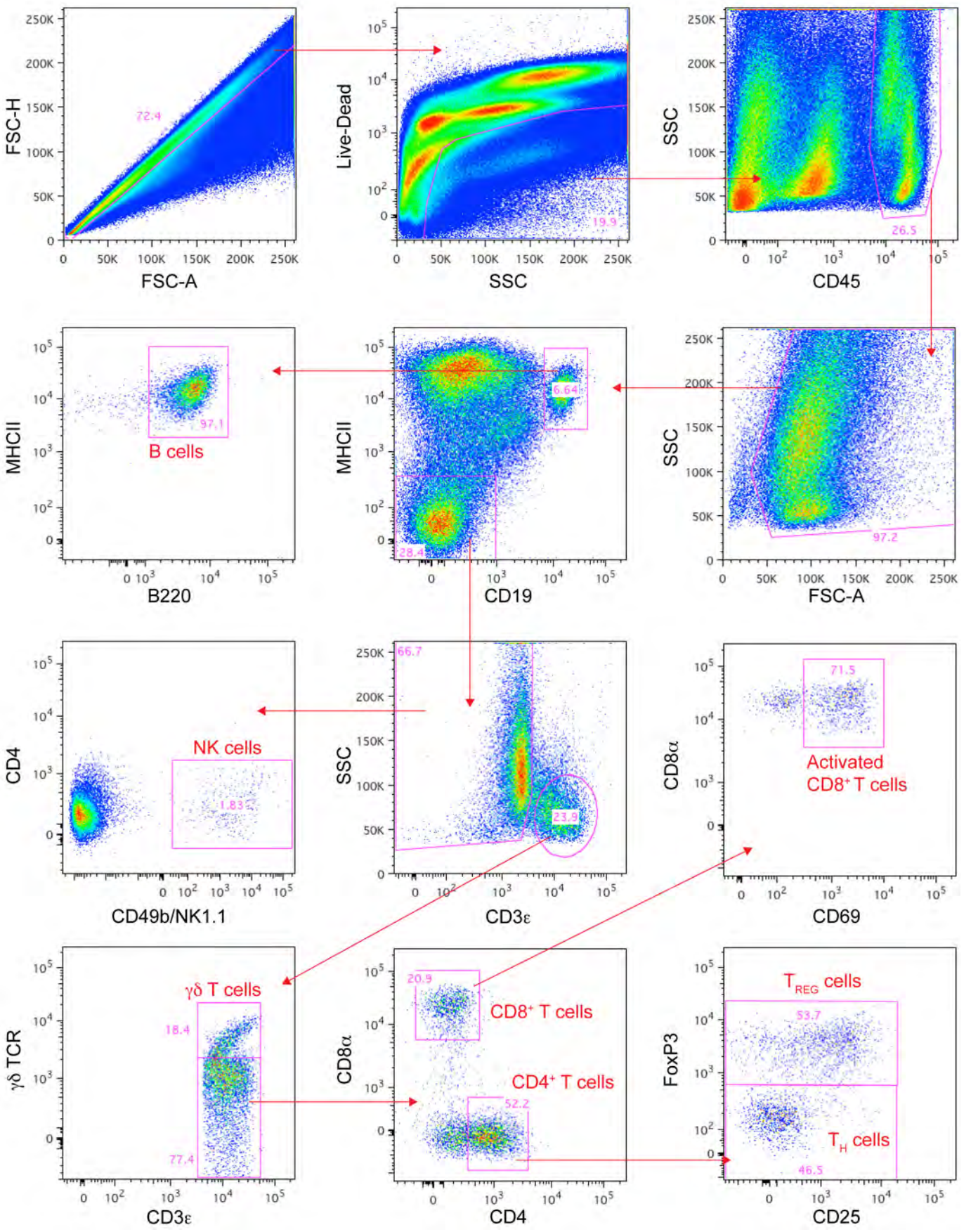
Cancer Cell, Volume 26

Supplemental Information

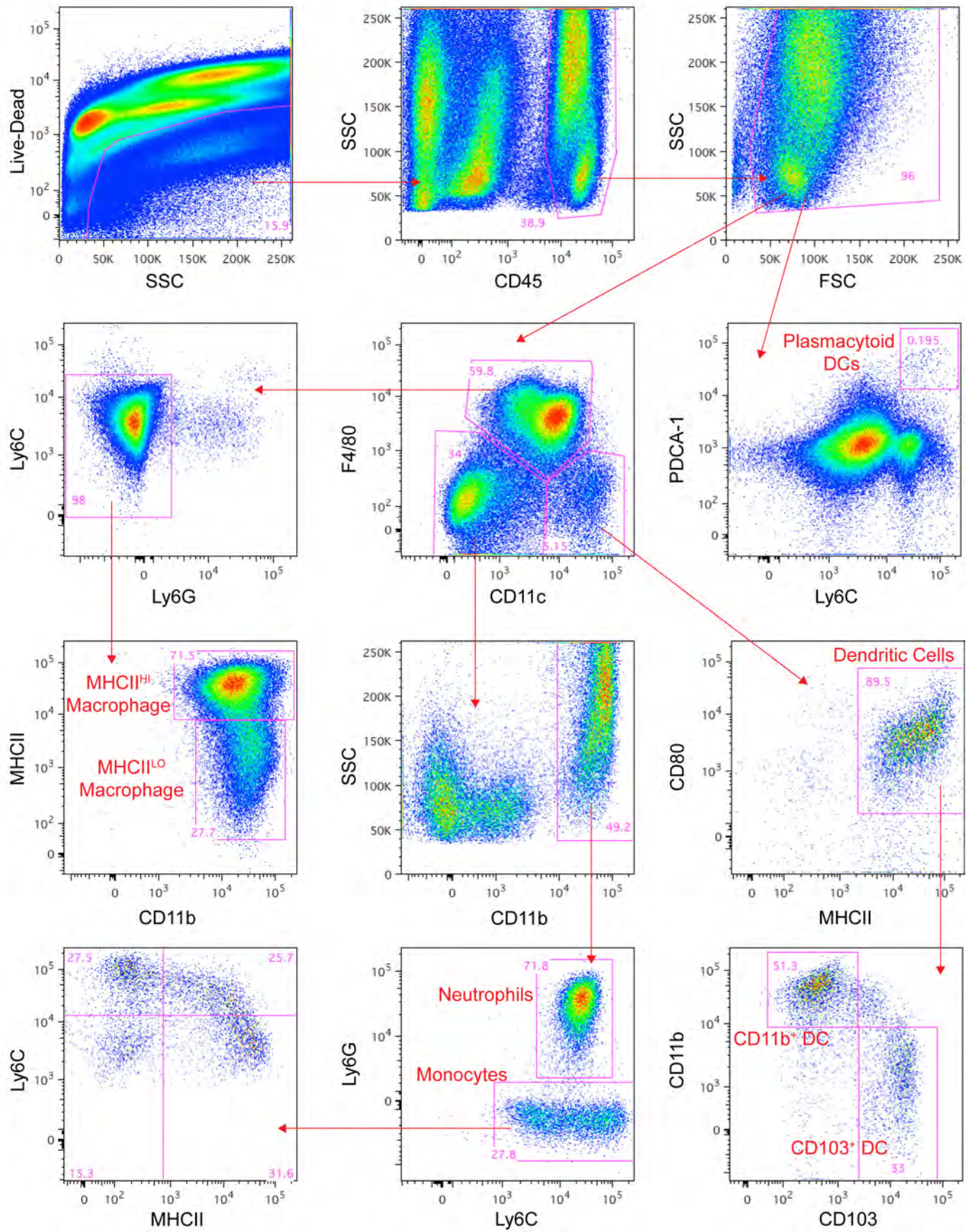
**Macrophage IL-10 Blocks CD8⁺ T Cell-Dependent
Responses to Chemotherapy by Suppressing IL-12
Expression in Intratumoral Dendritic Cells**

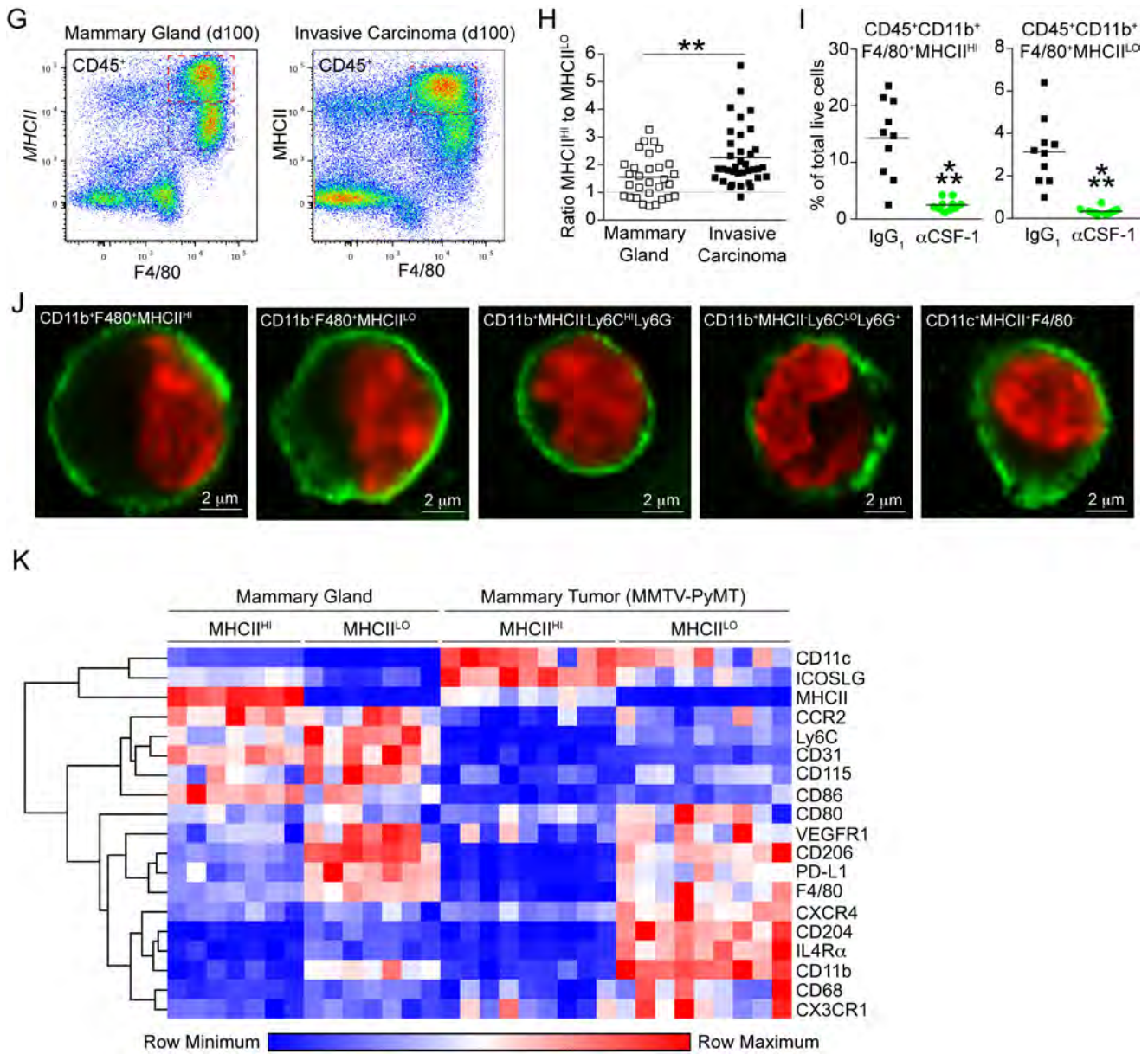
Brian Ruffell, Debbie Chang-Strachan, Vivien Chan, Alexander Rosenbusch, Christine M.T. Ho, Nancy Pryer, Dylan Daniel, E. Shelley Hwang, Hope S. Rugo, and Lisa M. Coussens

F



F





L

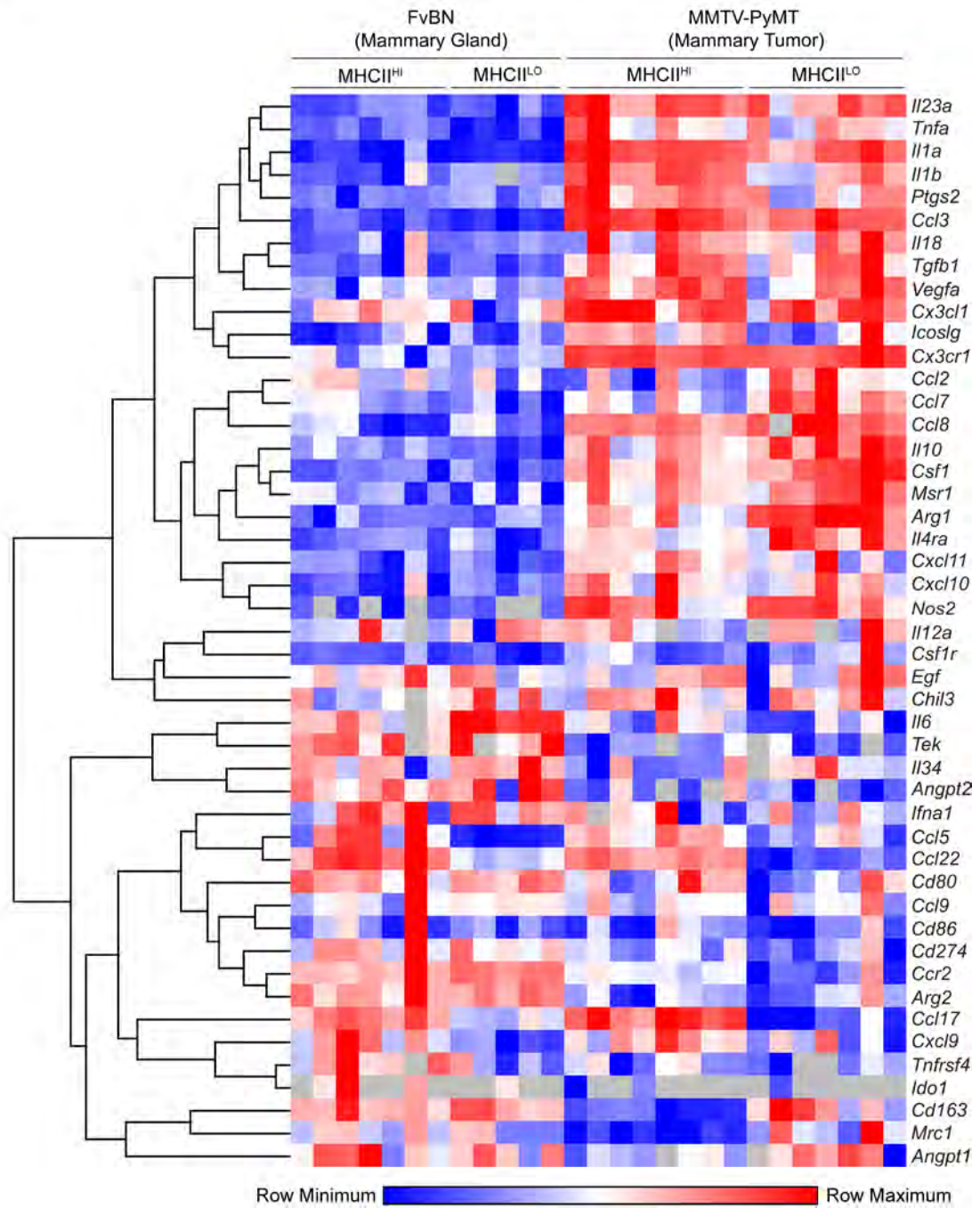


Figure S1, related to Figure 1: (A) Representative images of CD31 immunoreactivity (left panels) with quantitation of vessel density (right panel) for mammary tumors from MMTV-PyMT mice treated with IgG₁ control or α CSF-1 mAb for 20 days. (B) Representative immunofluorescent images displaying CD31 (white), desmin (green) and α -smooth muscle actin (red) staining in mammary tumors of MMTV-PyMT mice treated for 20 days. The ratio of pericytes (EpCAM⁻CD45⁻PDGFR α ⁻Desmin/SMA⁺) to endothelial cells (CD31^{HI}CD45⁻EpCAM⁺), as determined by flow cytometry, is shown to the right. (C) Uptake of doxorubicin 30 minutes post i.v injection in MMTV-PyMT mice treated for 10 days with IgG₁ control or α CSF-1. Representative confocal images are shown to the left with FITC-lectin marking the vasculature in green and doxorubicin fluorescence shown in red. Quantitation of doxorubicin fluorescence is shown to the right compared to non-injected controls. Data is displayed as mean \pm SEM with $n \geq 3$ mice per group. Significance determined by unpaired *t*-test with Welch's correction. (D) Pharmacokinetics of paclitaxel in mice bearing orthotopic MMTV-PyMT tumors treated with IgG₁ control (circles) or α CSF-1 mAb (triangles) for 10 days. Concentration of paclitaxel (ng/ml of plasma or tissue homogenate) is shown for plasma (red), tumors (blue) and liver (green) up to 8 hours post i.v. injection. Data is displayed as mean \pm SEM with $n \geq 5$ mice per time point. (E) Gating strategy for the identification of lymphoid-lineage populations. Starting from the upper left, arrows indicate directionality of sub-gates. Markers are indicated to the left and bottom of each polychromatic dot plot. Identified populations are marked in red text. (F) Gating strategy for identification of myeloid-lineage populations. Starting from the upper left, arrows indicate directionality of sub-gates. Markers are indicated to the left and bottom of each polychromatic dot plot. Identified populations are marked in red text. (G) Flow cytometry plots of CD45⁺ cells displaying expression of MHCII and F4/80 in mammary glands and MMTV-PyMT mammary carcinomas at 100 days of age. Dotted boxes display gating used to define MHCII^{HI} and MHCII^{LO} populations for B-F. (H) Ratio of MHCII^{HI} to MHCII^{LO} macrophages in mammary glands and mammary carcinomas in sets of age matched mice between days 100-110. Significance determined by unpaired *t*-test with ****p < 0.01**. (I) Infiltration by MHCII^{HI} (left) and MHCII^{LO} (right) macrophages in mammary tumors from MMTV-PyMT animals treated with IgG₁ or α CSF-1 mAb for 20 days determined by flow cytometry and shown as a percent of total live cells. Significance determined by unpaired *t*-test with Welch's correction, with *****p < 0.001**. (J) Confocal microscopy images of FACS-sorted populations from MMTV-PyMT mammary tumors stained with β -actin (green) and DAPI (red). (K) Relative expression of cell surface markers on macrophage subsets determined by flow cytometry using mean fluorescence intensity. Data is displayed as a heat map with hierarchical clustering. CD115 expression levels were measured by intracellular staining. (L) Relative gene expression in macrophage subsets determined by real time PCR. Data is displayed as a heat map with hierarchical clustering. Genes undetectable in select populations are displayed in gray.

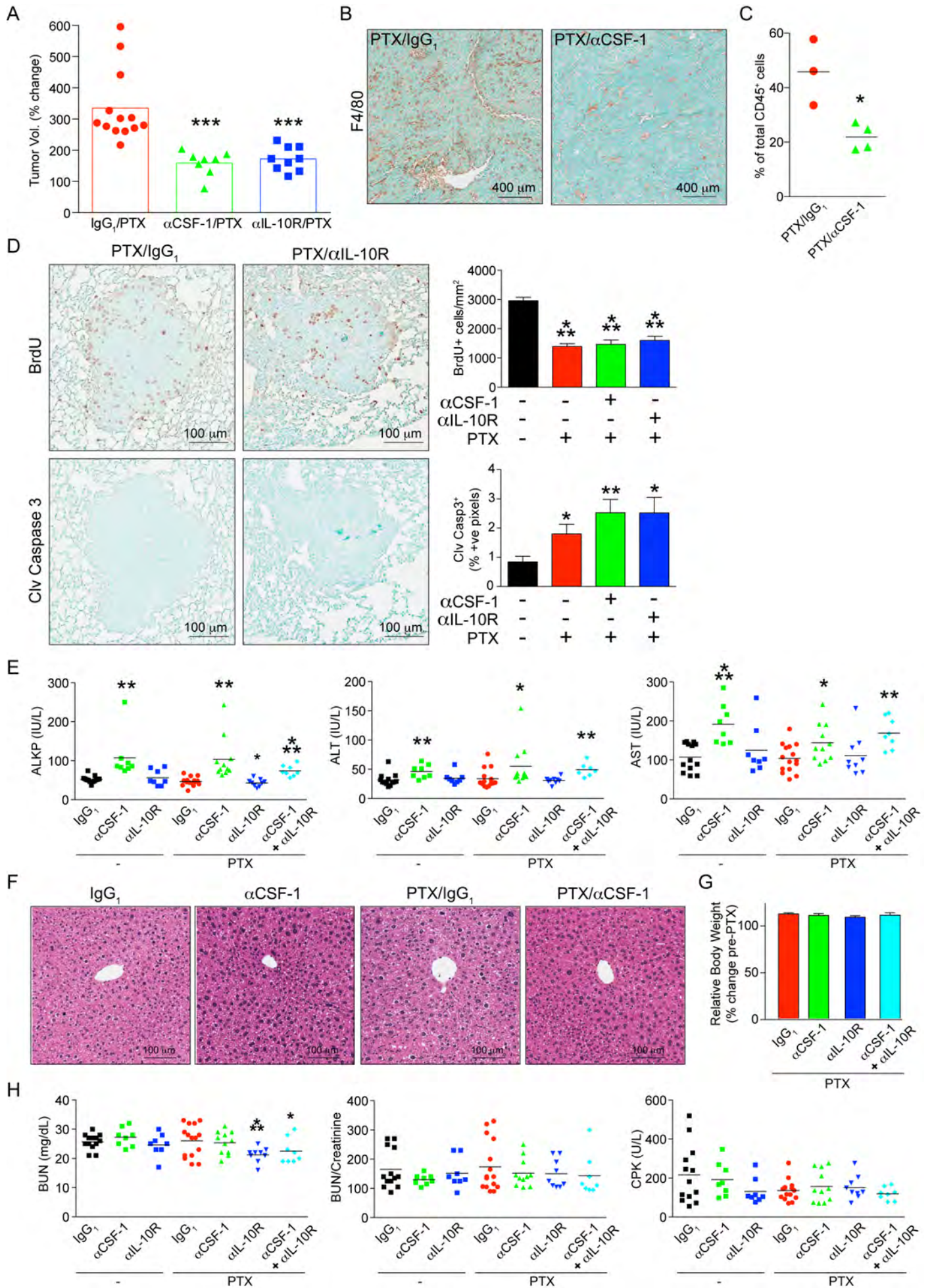


Figure S2, related to Figure 2: (A) Relative tumor volume after 3 rounds of PTX in C3(1)-TAg transgenic mice following combination therapy with α CSF-1 mAb or α IL-10R mAb. Significance determined by unpaired *t*-test with Welch's correction with *** $p < 0.001$. (B) F4/80 immunohistochemistry in C3(1)-TAg tumors following treatment with PTX in combination with IgG₁ or α CSF-1 mAb. (C) Percent of total CD45⁺ cells in C3(1)-TAg tumors comprised of CD11b⁺F4/80⁺MHCII⁺Ly6C⁻ macrophages. Data generated by flow cytometry. Significance determined by an unpaired *t*-test with * $p < 0.05$. (D) Proliferation (BrdU positivity) and cell death (cleaved caspase 3 positivity) in metastatic foci of MMTV-PyMT animals treated with combinatorial chemotherapy. Representative images are shown on left, with quantitation shown on right. Data is displayed as mean \pm SEM with $n \geq 9$ mice per group. Significance determined by unpaired *t*-test with Welch's correction with * $p < 0.05$, ** $p < 0.01$, *** $p < 0.001$. (E) Liver function tests based on serum isolated from MMTV-PyMT transgenic mice treated with combinatorial CTX. Significance determined by an unpaired *t*-test with Welch's correction with * $p < 0.05$, ** $p < 0.01$, *** $p < 0.001$. (F) Representative H&E sections of liver from mice in A with no evidence of tissue pathology. (G) Percent change in body weight following 3 doses of PTX in the different treatment groups. Data is displayed as mean \pm SEM. (H) Renal function tests (BUN, BUN/Creatinine) and CPK measurements for muscle damage in serum of mice. Significance determined by unpaired *t*-test with Welch's correction with * $p < 0.05$, ** $p < 0.01$.

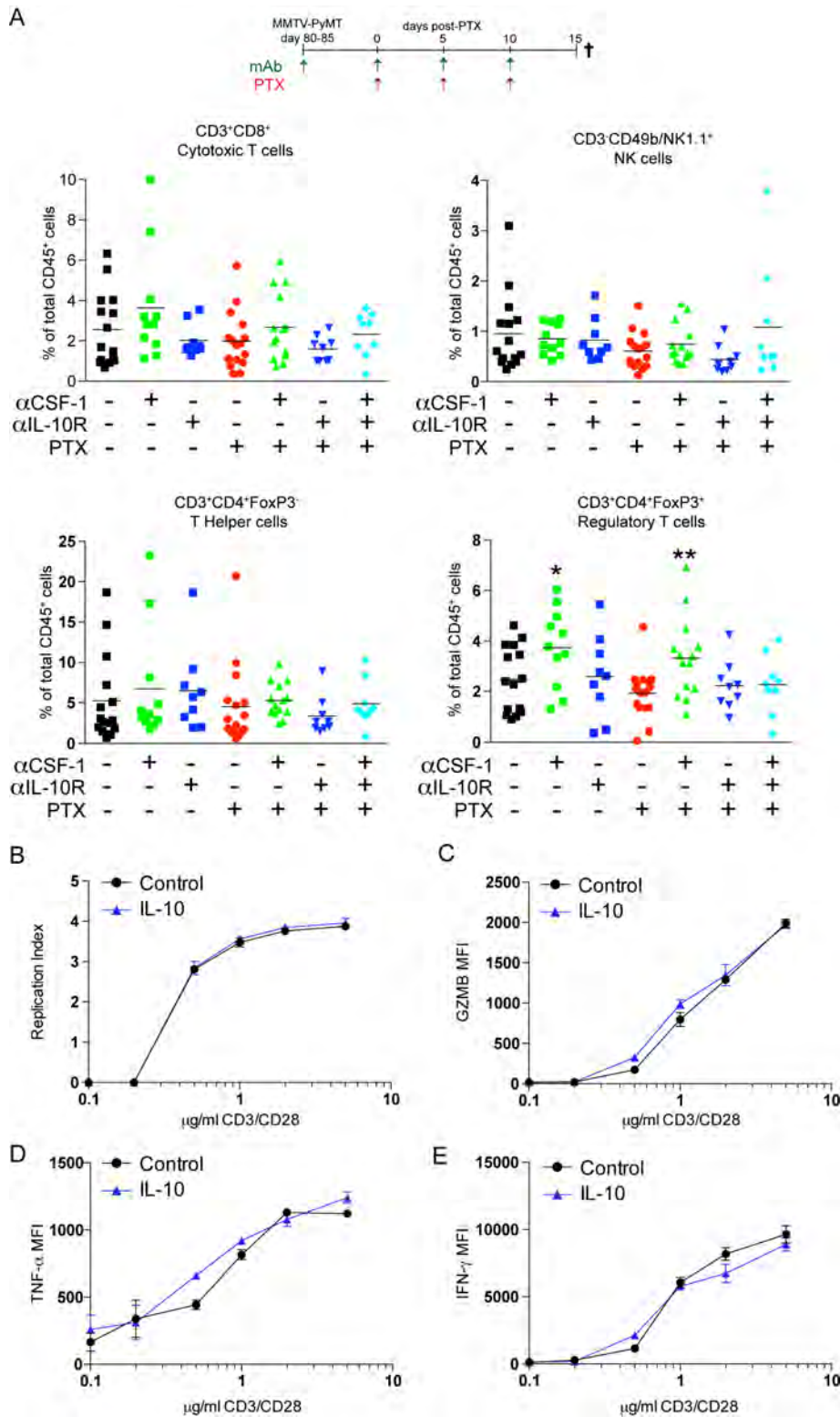


Figure S3, related to Figure 3: (A) Immune populations within the tumors of MMTV-PyMT animals treated with 3 rounds of PTX were identified via polychromatic flow cytometry and are displayed as a percentage of total CD45⁺ cells. Significance is shown compared to the IgG₁ control group for PTX-naïve mice and to the PTX/IgG₁ group for PTX-treated mice, and was determined by an unpaired *t*-test **p* < 0.05, ***p* < 0.01, ****p* < 0.001. (B-E) Purified splenic CD8⁺ T cells were stimulated with α CD3/ α CD28 for 48 hrs in the presence of 10 ng/ml IL-10 and measured for fold expansion by replication index (A), expression of GZMB (B), expression of TNF- α (C), or expression of IFN- γ (D). Samples were assayed in triplicate and one of three representative experiments is shown. Data is displayed as mean \pm SEM.

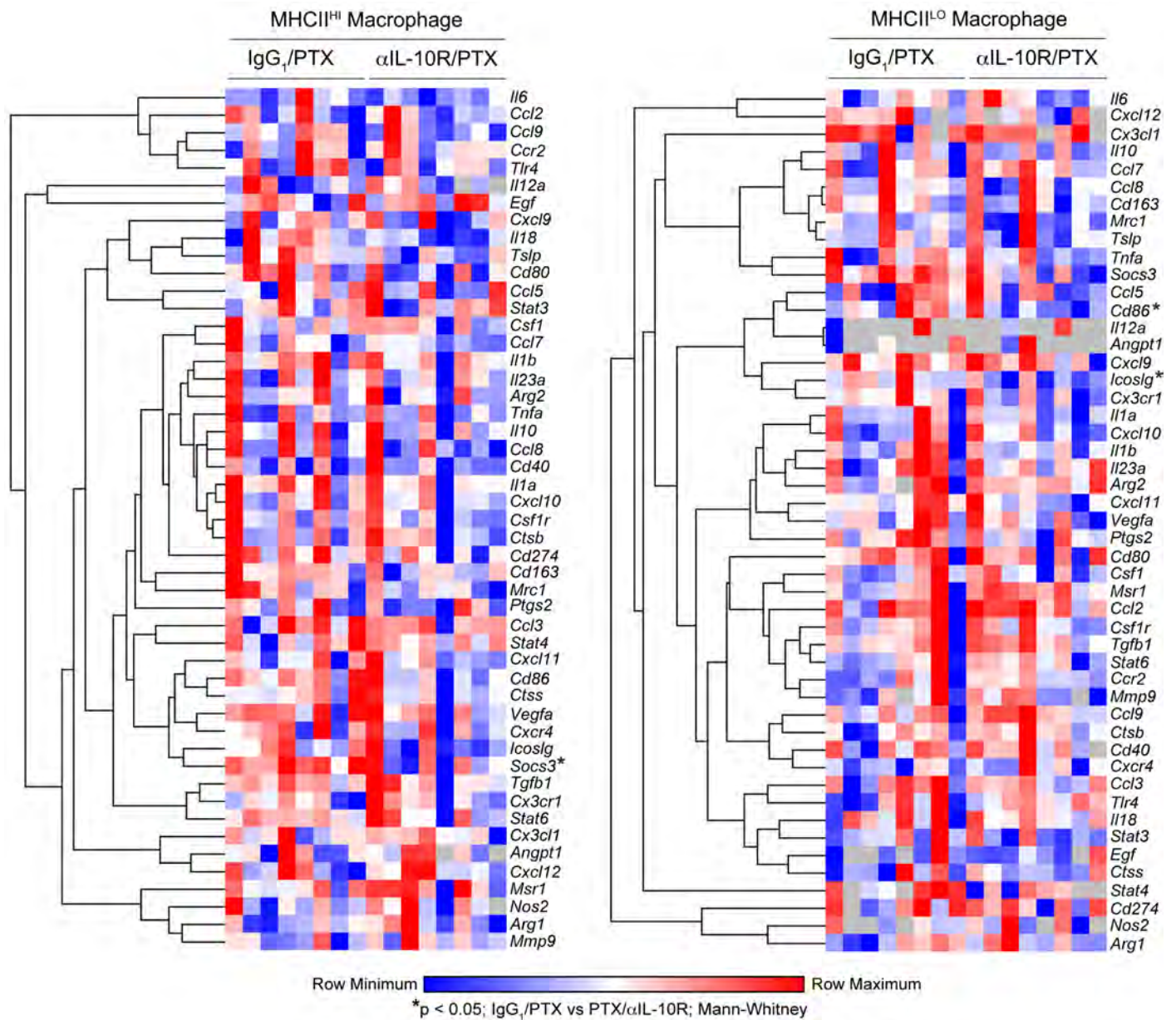


Figure S4, related to Figure 4: Gene expression by real time PCR in MHCII^{HI} and MHCII^{LO} macrophage subsets isolated from MMTV-PyMT animals treated with IgG₁/PTX or αIL-10R/PTX. Data was analyzed by comparative threshold cycle method using *Tbp* as a reference gene and is represented by a heat map with hierarchical clustering. Genes undetectable in select populations are displayed in gray. Significance determined by Mann-Whitney with *p < 0.05.

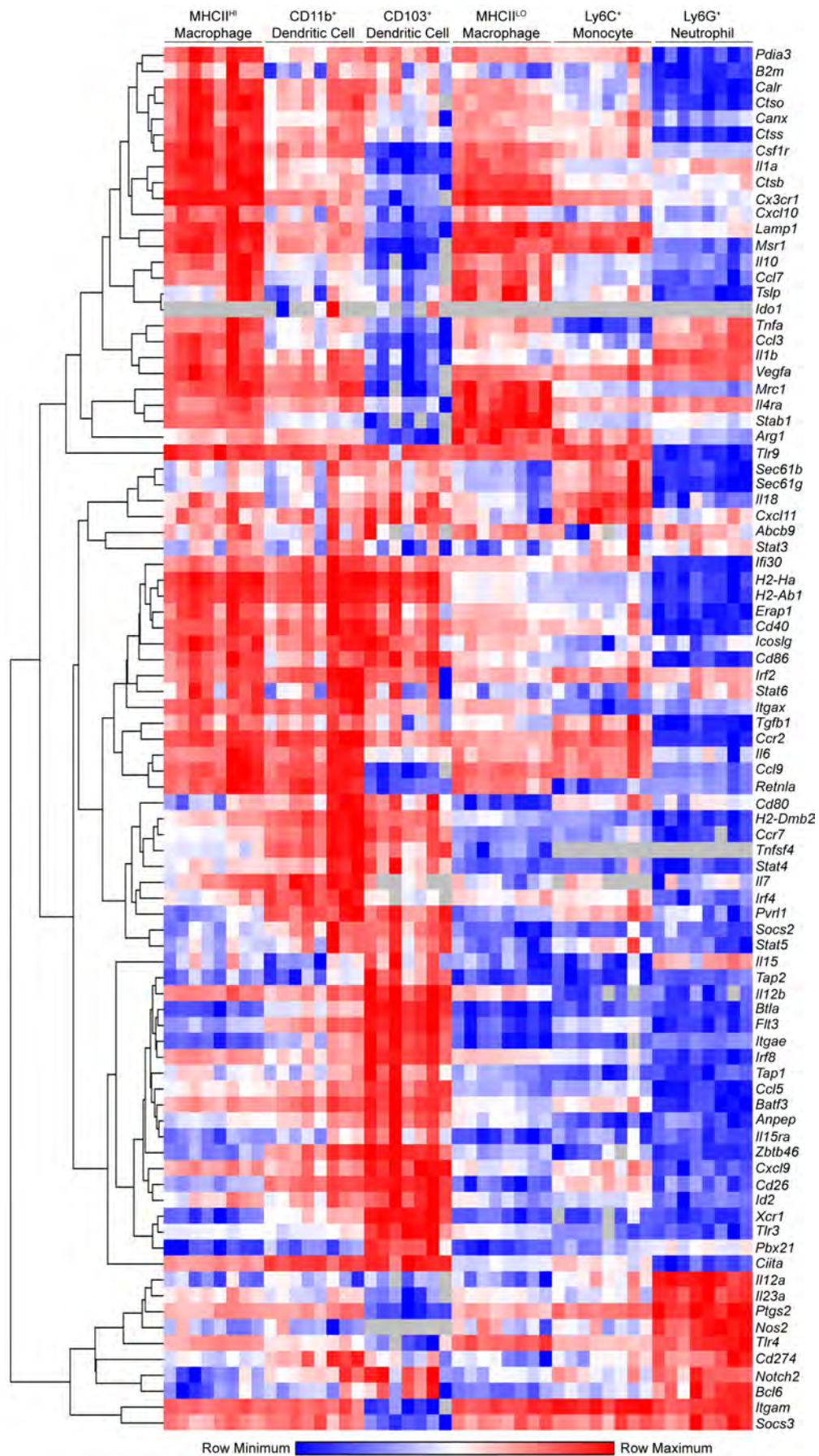


Figure S5, related to Figure 5: Real time PCR analysis of FACS-sorted myeloid populations from mammary tumors of untreated, end-stage MMTV-PyMT mice (>100 days). Data is displayed as a heat map with hierarchical clustering. Genes undetectable in select populations are displayed in gray.

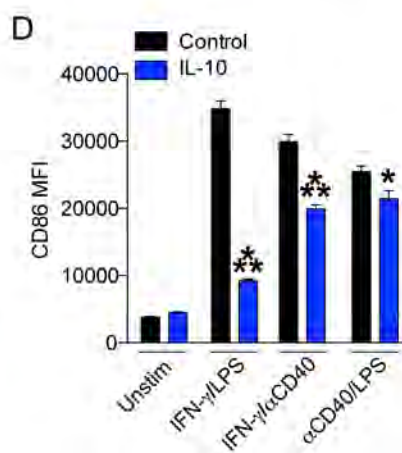
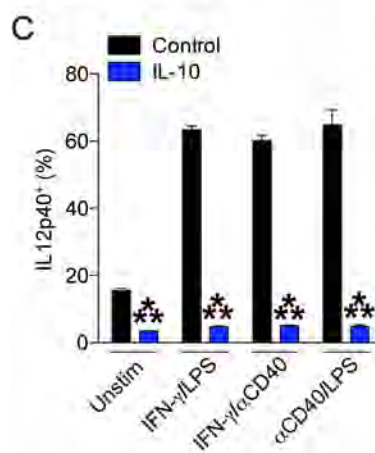
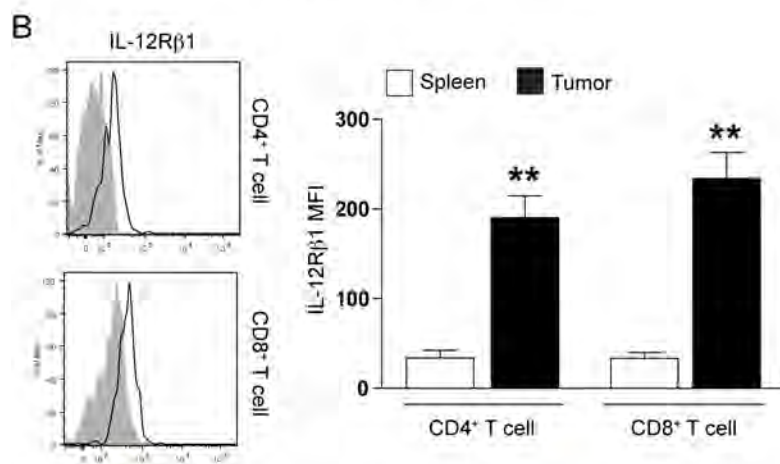
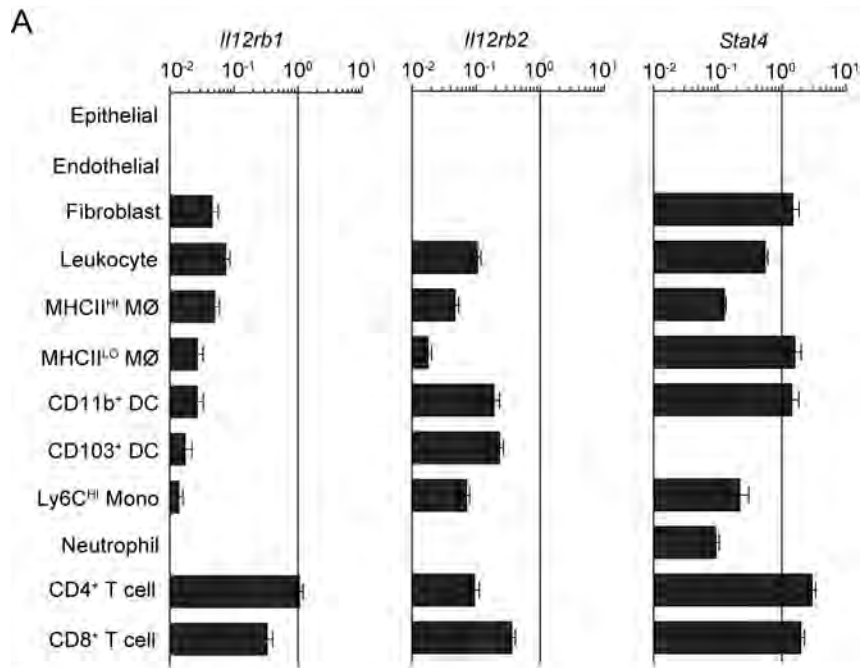


Figure S6, related to Figure 6: (A) Real time PCR analysis of *Il12rb1*, *Il12rb2*, and *Stat4* from FACS-sorted leukocyte populations from the tumors of untreated, end-stage MMTV-PyMT mice (>100 days). Data is normalized to *Tbp* expression and is displayed as mean \pm SEM with n=8 mice per cell type. MØ, macrophage; mono, monocyte; DC, dendritic cell. (B) Surface expression of IL12R β 1 as measured by mean fluorescence intensity (MFI) minus background in T lymphocytes from MMTV-PyMT mammary tumors and normal spleens. Data is displayed as mean \pm SEM with n=4 mice per group. Significance was determined by an unpaired *t*-test with ***p* < 0.01. Representative histograms of T lymphocytes from MMTV-PyMT mammary tumors are shown to the left. (C) Percent of BMDCs expressing IL-12p40 by intracellular flow cytometry following 24 hr stimulation with IFN- γ /LPS, IFN- γ / α CD40 or α CD40/LPS. Cells were pre-treated for 24 hours with 10 U/ml IL-10 prior to stimulation. (D) Surface expression of CD86 on the BMDCs from C, as determined by mean fluorescence intensity. For C-D, samples were assayed in quadruplicate and one of two representative experiments is shown. Data is displayed as mean \pm SEM. Significance determined by unpaired *t*-test relative the control group, with **p* < 0.05, ****p* < 0.001.

SUPPLEMENTAL EXPERIMENTAL PROCEDURES

Quantitation of metastatic burden

Following resection, lungs from transgenic MMTV-PyMT animals were injected with neutral buffered formalin via the trachea and incubated overnight in formalin prior to ethanol dehydration and paraffin embedding. Lungs were sectioned and haematoxylin and eosin staining was performed on slides throughout lungs stationed 100 μm apart for analysis. Frequency and size of the metastatic foci were determined by manual circling in a blinded fashion using Imagescope software.

Flow cytometry and fluorescence activated cell sorting

Isolation and staining of stromal cell populations was performed as described using antibodies from BioLegend and eBioscience (Ruffell et al., 2013). Ex vivo intracellular staining (Liu and Whitton, 2005) for IL-12p40 was performed on isolated cells 6 hours following an intravenous injection of 0.25 mg brefeldin A (Sigma-Aldrich). Gating strategies can be found in supplemental Figure S2-3. For flow cytometry, data was collected with either a LSRII or Fortessa flow cytometer (BD Bioscience) with analysis performed using FlowJo (Tree Star Incorporated). Fluorescent-activated cell sorting (FACS) was conducted on a FACSariaII or InFlux (BD Biosciences). Sorted cells were either used immediately in vitro or flash frozen in liquid nitrogen as a cell pellet for subsequent gene expression analysis.

Real-time PCR

Mice were cardiac-perfused to clear peripheral blood. Tumor tissues were snap-frozen and pulverized in liquid nitrogen for whole tissue analysis, or were used to purify immune populations by FACS. Total mRNA was prepared using RNeasy Micro/Mini kit guidelines (Qiagen) followed by RNA quantitation using a NanoDrop ND-1000 (Thermo Fisher Scientific). Contaminating DNA was removed with DNase I (Life Technologies), and then SuperScript III (Life Technologies) was used to reverse transcribe purified RNA into cDNA according to manufacturer's directions. Real-time PCR for gene expression was performed using individual TaqMan Assays or microfluidic TaqMan Low Density Arrays (Life Technologies). A preamplification step (Life Technologies) was used prior to analysis of FACS-sorted populations. The comparative threshold cycle method was used to calculate fold change in gene expression, which was normalized to either a single (*Tbp*) or multiple (*Actb*, *Gusb*, *Gapdh*, *Pgk1*, *Tfrc*) reference genes.

Immunohistochemistry

Immunohistochemistry was performed as described for mouse (Ruffell et al., 2013) and human tissue (Ruffell et al., 2012). Citrate retrieval was used for BrdU (BU1/75; 1:200; Serotec), cleaved Caspase 3 (1:200; Cell Signaling), granzyme B (1:200; Novus Biologicals), and IL-10 (1:100; R&D Systems). Proteinase K retrieval (Dako) was used for CD31 (MEC13.3; 1:100; eBioscience) and F4/80 (CI:A3-1;

1:500; Serotec). All slides were digitally scanned using the Aperio ScanScope CS Slide Scanner with a 20X objective. Automated quantitative image analysis was performed using Imagescope (Aperio) and the provided positive pixel (cleaved caspase 3) or nuclear stain (BrdU) detection algorithm. CD31 and granzyme B quantitation was done by manual counting in a blinded fashion.

Immunofluorescence

Animals were injected intravenously with 8.0 mg/kg doxorubicin and 100 μ l of 1.0 mg/ml fluorescein-labeled *Lycopersicon esculentum* Lectin (Tomato Lectin, Vector Laboratories) for 30 min and 3 min, respectively, prior to cardiac perfusion with PBS containing 4% paraformaldehyde (PFA, Electron Microscopy Sciences) and embedding tissue into OCT. Alternatively, animals were cardiac perfused with PBS containing 10 U/ml of Heparin and tissue was directly embedded into OCT. Unfixed tumors were permeabilized with 100% ice-cold acetone for 10 min, washed in PBS, and then blocked with goat blocking buffer for 1 hr. Primary antibodies including α -smooth muscle actin Cy3 (1:1000, Sigma), desmin (1:500, Millipore/Upstate), CD31 (1:100, BioLegend), F4/80 (1:100, BioLegend), CD103 (1:100, BioLegend), and pan-Keratin (1:100, Cell Signaling) were diluted in 0.5x blocking buffer and incubated on sections overnight at 4°C. For immunofluorescent staining of human breast cancer tissues, 5 μ m sections of formalin fixed, paraffin embedded tissue were deparaffinized with xylene, rehydrated, and subjected to antigen retrieval with heated citrate buffer (BioGenex). After 1 hr in horse serum blocking buffer, CD163 (1:50, Thermo Scientific) and IL-10 (1:100; R&D Systems) antibodies were applied overnight at 4°C. After washing, secondary antibodies from Life Technologies were used at 1:500 for 30 min at room temperature, followed by incubation with 1.0 μ g/ml Hoechst 33342 (Life Technologies) for 15 min. Slides were then washed and mounted with ProLong Gold anti-fade mounting medium (Life Technologies). Sorted cells were affixed to slides by a Shandon Cytospin, fixed/permeabilized with 100% ethanol, and then stained for β -actin (1:1000; Sigma-Aldrich) as described above except with the use DAPI as a nuclear stain. Images were taken with a LSM510 Confocal Laser Scanning microscope (Carl Zeiss), Nikon C1si Spectral Confocal Microscope, or Ariol automated scanning microscope (Leica). Fluorescent quantitation was performed with ImageJ.

Flt-3 Ligand Bone Marrow DCs

Bone marrow was harvested from FVB/n female mice and red blood cells lysed with Pharmlyse (BD Biosciences). Remaining cells were plated at 2×10^6 per ml in RPMI1640 containing 2.0 mM L-glutamine and 25 mM HEPES, supplemented with 10 mM Sodium Pyruvate, nonessential amino acids, 100 U/ml penicillin/streptomycin, 55 μ M B-ME, and 10% fetal calf serum (Life Technologies). Recombinant human Flt-3 Ligand Immunoglobulin (Flt-3L-Ig; BioXCell) was added at 100 ng/ml and cells were incubated untouched for 9 days. Cells in suspension were removed by pipetting (>90% CD11c⁺), resuspended at 10^6 per ml in RPMI1640 with 100 ng/ml Flt-3L-Ig, and incubated for 24 hours with 1.0-10 U/ml IL-10 (Peprotech). Cells were then stimulated for an additional 24 hours with a combination of IFN- γ (40 ng/ml;

Peptrotech), LPS-EB Ultrapure (100 ng/ml; InvivoGen), or α CD40 (10 μ g/ml; FGK4.5; BioXCell). For intracellular flow cytometry, Brefeldin A (3.0 μ g/ml; eBioscience) was added 4 hours prior to harvesting the cells.

T cell activation

Splenic CD8⁺ T cells were purified by magnetic negative selection (Stem Cell Technologies) to over 95% purity and labeled with Cell Trace Violet (Invitrogen). CD8⁺ T cells (10^5) were then placed in a 96-well plate coated with 5.0 μ g/ml α CD3 (145.2C11) and α CD28 (PV-1) antibodies in RPMI1640 containing 2.0 mM L-glutamine and 25 mM HEPES, supplemented with 10 mM Sodium Pyruvate, 100 U/ml penicillin/streptomycin, 55 μ M B-ME, and 10% fetal calf serum (Life Technologies) for 48 hrs at 37°C. Brefeldin A (3.0 μ g/ml; eBioscience) was added 4 hours prior to harvesting the cells for intracellular staining with GZMB PE, IFN- γ APC, and TNF- α PE-Cy7. Data acquisition was performed on a BD Fortessa flow cytometer with analysis using FlowJo software.

T cell suppression assay

Splenic CD8⁺ T cells were purified by magnetic negative selection (Stem Cell Technologies) to over 95% purity and labeled with Cell Trace Violet (Invitrogen). CD8⁺ T cells (10^5) were then placed in a 96-well plate coated with 5 μ g/ml α CD3 (145.2C11) and α CD28 (PV-1) antibodies. After a brief spin, FACS-sorted macrophages from MMTV-PyMT late stage tumors were added into wells at various ratios with or without 10 μ g/ml of blocking/neutralizing antibodies. Cells were cultured together in RPMI1640 containing 2.0 mM L-glutamine and 25 mM HEPES, supplemented with 10 mM Sodium Pyruvate, 100 U/ml penicillin/streptomycin, 55 μ M B-ME, and 10% fetal calf serum (Life Technologies) for 60 hrs at 37°C. Cells were then stained with CD8-PE, CD11b-APC and 7AAD prior to analysis on an LSRII or Fortessa flow cytometer. The replication index was determined using FlowJo software.

Quantitation of paclitaxel

Mice bearing orthotopic mammary tumors were intravenously injected with 10 mg/kg paclitaxel and, following a cardiac puncture blood draw, were perfused to clear peripheral blood. Tumor and liver tissues were snap-frozen in liquid nitrogen. Liquid chromatography-mass spectrometry was performed on homogenized samples by Integrated Analytical Solutions (Berkeley, CA) using the injected compound as a reference sample.

Supplemental References

Liu, F., and Whitton, J. L. (2005). Cutting edge: re-evaluating the in vivo cytokine responses of CD8+ T cells during primary and secondary viral infections. *J Immunol* *174*, 5936-5940.

Ruffell, B., Affara, N. I., Cottone, L., Junankar, S., Johansson, M., DeNardo, D. G., Korets, L., Reinheckel, T., Sloane, B. F., Bogyo, M., and Coussens, L. M. (2013). Cathepsin C is a tissue-specific regulator of squamous carcinogenesis. *Genes Dev* *27*, 2086-2098.